



HAL
open science

Application of pyridine-modified chitosan derivative for simultaneous adsorption of Cu(II) and oxyanions of Cr(VI) from aqueous solution

Fernanda Jorge Gonçalves, L. V. A. Alves Gurgel, Liliane Catone Soares, Filipe Simões Teodoro, Guilherme Max Dias Ferreira, Yara Luíza Coelho, Luis Henrique Mendes da Silva, Damien Prim, L. F. Gil

► To cite this version:

Fernanda Jorge Gonçalves, L. V. A. Alves Gurgel, Liliane Catone Soares, Filipe Simões Teodoro, Guilherme Max Dias Ferreira, et al.. Application of pyridine-modified chitosan derivative for simultaneous adsorption of Cu(II) and oxyanions of Cr(VI) from aqueous solution. *Journal of Environmental Management*, 2021, 282, 10.1016/j.jenvman.2021.111939 . hal-03171221

HAL Id: hal-03171221

<https://hal.science/hal-03171221>

Submitted on 28 Mar 2021

HAL is a multi-disciplinary open access archive for the deposit and dissemination of scientific research documents, whether they are published or not. The documents may come from teaching and research institutions in France or abroad, or from public or private research centers.

L'archive ouverte pluridisciplinaire **HAL**, est destinée au dépôt et à la diffusion de documents scientifiques de niveau recherche, publiés ou non, émanant des établissements d'enseignement et de recherche français ou étrangers, des laboratoires publics ou privés.

1 **Application of pyridine-modified chitosan derivative for simultaneous adsorption of**
2 **Cu(II) and oxyanions of Cr(VI) from aqueous solution**

3 Fernanda Jorge Gonçalves^a, Leandro Vinícius Alves Gurgel^a, Liliane Catone Soares^a,
4 Filipe Simões Teodoro^a, Guilherme Max Dias Ferreira^b, Yara Luiza Coelho^c, Luis
5 Henrique Mendes da Silva^c, Damien Prim^d, Laurent Frédéric Gil^{a,*}

6 ^a Environmental Organic Chemistry Group, Department of Chemistry, Institute of
7 Biological and Exact Sciences, Federal University of Ouro Preto, Campus Universitário
8 Morro do Cruzeiro, Bauxita, Ouro Preto 35400-000, Minas Gerais, Brazil

9 ^b Department of Chemistry, Federal University of Lavras (UFLA), Campus Universitário,
10 Lavras 37200-000, Minas Gerais, Brazil

11 ^c Colloidal and Macromolecular Green Chemistry Group, Department of Chemistry,
12 Federal University of Viçosa, Av. P.H. Rolfs, s/nº, Viçosa 36570-000, Minas Gerais,
13 Brazil

14 ^d University of Versailles St-Quentin-en-Yvelines, Institut Lavoisier de Versailles UMR
15 CNRS 8180, 45, avenue des Etats-Unis, 78035 Versailles, France

16 *Corresponding author. Tel.: +55 31 3559 1707; fax: +55 31 3559 1707; E-mail address:
17 laurent@ufop.edu.br_(L. F. Gil)

18

19 **Abstract**

20 The bioadsorbent **C1**, which is a chitosan derivative prepared in a one-step synthesis, was
21 successfully used to adsorb Cr(VI) and Cu(II) simultaneously. Here, for the first time the
22 simultaneous adsorption of a cation and an anion was modeled using the Corsel model
23 for kinetics and the Real Adsorbed Solution Theory model for equilibrium data. Batch
24 studies of the adsorption of Cu(II) and Cr(VI) in single and binary aqueous solutions were
25 performed as a function of initial solute concentration, contact time, and solution pH.
26 Here, for the first time the simultaneous adsorption of a cation and an anion was modeled
27 using the Corsel model for kinetics and Real Adsorbed Solution Theory model for
28 equilibrium data. The maximum adsorption capacities of **C1** in single and binary aqueous
29 solutions were 1.84 and 1.13 mmol g⁻¹ for Cu(II) and 3.86 and 0.98 mmol g⁻¹ for Cr(VI),
30 respectively. The reuse of **C1** was investigated, with Cu(II) ions being almost completely
31 desorbed and fully re-adsorbed. For Cr(VI), the desorption was incomplete resulting in a
32 lower re-adsorption. Energy-dispersive X-ray spectroscopy was used for mapping the
33 distributions of Cr(VI) and Cu(II) adsorbed on the **C1** surface in single and binary
34 adsorption systems. Isothermal titration calorimetry experiments were performed for
35 Cr(VI) and Cu(II) adsorption in single solutions. The thermodynamic parameters of
36 adsorption showed that the adsorption of both metal ions was enthalpically driven, but
37 entropically unfavorable.

38 **Keywords:** one-step synthesis; pyridine-2-carbaldehyde; copper; chromium; Real
39 Adsorbed Solution Theory, Corsel model.

40 **1. Introduction**

41 Many environmental and public health problems are related to the contamination of water
42 resources (Li et al., 2015; Purkayastha et al., 2014; Wu et al., 2018). Metals are often
43 found as major contaminants of aquatic systems, and can be highly toxic to humans and
44 animals (Teodoro et al., 2016; Uddin, 2017; Xin et al., 2017). The main causes of
45 contamination of water by toxic metals include industrial activities such as the
46 manufacture of batteries, textiles, paints, and pesticides, as well as petroleum refining and
47 mining operations (O'Connell et al., 2008; Ramos et al., 2015). The toxic metals
48 discharged by industries include cadmium, mercury, lead, chromium, copper, nickel, and
49 zinc (Wan Ngah et al., 2011).

50 Copper is widely used in electrical materials, alloys, fungicides, and herbicides, and is
51 associated with industrial wastes, mining activities, and power generation (Ayres et al.,
52 2003). High concentrations of copper lead to health impacts including chronic or acute
53 liver disease, neurological problems, and psychiatric disorders such as Wilson's disease
54 (Mulligan and Bronstein, 2020). Chromium is used in stainless steel and alloys, chrome
55 plating, leather tanning, dyes and pigments, and wood preservation (Morrison and
56 Murphy, 2010). Cr(VI) is toxic and a well-known human carcinogenic. It causes damage
57 to the immune, respiratory, gastrointestinal, reproductive, and hematological systems
58 (Wilbur et al., 2012).

59 Cr(VI) and Cu(II) are common ions and generally coexist in wastewater, notably in
60 discharges from the electroplating and tanning industries. For example, Sarkar et al.
61 (2015) showed concern to analyze the concentrations chromium and copper in the
62 Buriganga river (Bangladesh) due to the pollution caused by the tannery effluent. In
63 addition to the tannery industry, copper is also emitted from the sewage pipe lines (Sarkar
64 et al., 2015). Regarding this kind of waste, some works reported the use of photoreduction

65 (Yan et al., 2020) and adsorption on carbonized crofton weed (Chen et al., 2016) and
66 hyacinth shoot powder (Sarkar et al., 2017) for simultaneous removal of Cr(VI) and
67 Cu(II). Copper and chromium are also present in the formulation of chromated copper
68 arsenate (CCA), a wood preservative to avoid attack by termites and fungi (ATSDR,
69 2011). CCA is no longer used for residential construction but it still used for industrial
70 and commercial constructions (NPIC, 2014). Since CCA is a water-soluble substance,
71 there is a concern about water and soil contamination by leaching from CCA-treated wood
72 (ATSDR, 2011).

73 Inefficient treatment of effluents contaminated with toxic metals in wastewater treatment
74 plants (WWTPs) can cause long-term risks to ecosystems and humans. Various
75 techniques have been used for removal of toxic metals in WWTPs, such as chemical
76 precipitation, flocculation and coagulation, oxidation/reduction, and nanofiltration (Mosa
77 et al., 2016; Purkayastha et al., 2014; Teodoro et al., 2016). Adsorption may be used as a
78 treatment or as a polishing technique in WWTPs, offering high efficiency and flexibility
79 of operation (Li et al., 2018; Silva-Yumi et al., 2018; Xin et al., 2017). As a polishing
80 technique, adsorption can be used to achieve drinking water standards. According to the
81 WHO, the provisional guideline values for Cr and Cu in drinking water are 0.05 and
82 2.0 mg L⁻¹, respectively (WHO, 1996a, b).

83 The availability of cost-effective, highly efficient, and environmentally friendly
84 adsorbents is extremely important for the feasibility of adsorption techniques applied to
85 treat water and wastewater (Rahimi et al., 2018; Silva-Yumi et al., 2018; Teodoro et al.,
86 2016). To this end, the use of adsorbents prepared from chemical modification of
87 biopolymers has attracted attention in recent years (Almeida et al., 2016; De Gisi et al.,
88 2016).

89 Polysaccharide-based biopolymers are a potential source of adsorbent materials.
90 Polysaccharides are widely found in nature, have varied molecular structures, and present
91 a wide range of physicochemical properties that can be exploited for different applications
92 (Kurita, 2001). Among the many types of natural polysaccharides, cellulose and chitin
93 are the most abundant (Ahmad et al., 2017; Almeida et al., 2016). Chitin is mainly isolated
94 from shrimp or lobster carapaces, as well as from the cell walls of some fungi (De Gisi et
95 al., 2016; Kurita, 2001). The partial deacetylation of chitin results in the formation of
96 chitosan, a polyaminosaccharide with glucose-like structures (2-amino-2-deoxy- β -D-
97 glucose and 2-acetamido-2-deoxy- β -D-glucose units) connected by $\beta(1\rightarrow4)$ linkages
98 (Ahmad et al., 2017; Kyzas et al., 2017). The presence of hydroxyl and free amine groups
99 in the chitosan structure provides excellent capacity of this material to act as a scavenger
100 of metal ions, so it is a promising starting material for the synthesis of different adsorbents
101 with improved properties (Divya and Jisha, 2018; Li et al., 2018; Wu et al., 2010). Several
102 recent studies have discussed the development of low-cost adsorbents based on
103 biopolymers such as chitosan, as an alternative to synthetic polymers (Ahmad et al., 2017;
104 De Gisi et al., 2016).

105 The aim of the present study was to model the simultaneous adsorption of a cation and an
106 anion using a versatile bioadsorbent. The present study is the first study to model the
107 simultaneous adsorption of a cation and an anion using the Corsel model for kinetics and
108 the Real Adsorbed Solution Theory (RAST) model for equilibrium data. These models
109 provide a more in-depth analysis of the interactions involved in the simultaneous
110 adsorption of Cu(II) and Cr(VI). It was employed a bioadsorbent, denoted **C1**, prepared
111 by modification of chitosan with pyridine-2-carbaldehyde (Goncalves et al. (2018). The
112 use of **C1** is relevant, because it was prepared using a one-step synthesis employing a

113 green solvent. **C1** was subsequently used to remove Cr(VI) and Cu(II) from single and
114 binary aqueous solutions.

115 Reuse of the spent adsorbent was also investigated. Isothermal titration calorimetry was
116 used to understand the differences between the adsorption of Cu(II) and oxyanions of
117 Cr(VI) on **C1**, with determination of the adsorption thermodynamic parameters.

118 **2. Material and methods**

119 **2.1. Material**

120 Chitosan (medium molecular weight, cat. no. 448877), pyridine-2-carbaldehyde,
121 $\text{CuSO}_4 \cdot 5\text{H}_2\text{O}$, and sodium chloroacetate (98%) were purchased from Sigma-Aldrich.
122 $\text{K}_2\text{Cr}_2\text{O}_7$, monochloroacetic acid (99%), $\text{CH}_3\text{COONa} \cdot 3\text{H}_2\text{O}$, Na_2CO_3 , anhydrous CaCl_2 ,
123 NaH_2PO_4 , Na_2HPO_4 , and ethylenediaminetetraacetic acid (EDTA) were purchased from
124 Synth (Brazil). Glycine was purchased from Isofar (Brazil). Glacial acetic acid (99.5%)
125 was purchased from Neon (Brazil). Ethyl alcohol (99.8%) was purchased from Dinâmica
126 (Brazil). HCl (37 wt.% in H_2O) was purchased from Vetec (Brazil). Filter paper
127 (quantitative, black ribbon, C-41, 12.5 cm diameter, 0.01% ash content, and grammage
128 of 85 g m^{-2}) was purchased from Unifil (Brazil).

129 The degree of acetylation (DA) of the chitosan was determined in a previous study of our
130 research group (Goncalves et al., 2018), using quantitative solid-state ^{13}C nuclear
131 magnetic resonance (SS ^{13}C NMR) spectroscopy. The estimated DA value of the chitosan
132 was $33 \pm 2\%$.

133 **2.2. Synthesis of C1**

134 The synthesis of **C1** was performed as described previously by Goncalves et al. (2018).
135 Chitosan (5 g) was added to a 500 mL round-bottom flask, together with 0.525 mols of
136 pyridine-2-carbaldehyde (50 mL) dissolved in 125 mL of ethyl alcohol (99.8%). A reflux
137 condenser with a drying tube filled with anhydrous CaCl_2 was attached to the flask. The
138 suspension was heated at 80.0 °C for 18 h, under gentle agitation (300 rpm) in an oil bath
139 (Model PC-420, Corning®). Subsequently, the cooled suspension was filtered under
140 reduced pressure, using a sintered glass funnel (porosity 3), followed by washing with
141 ethyl alcohol (95%), distilled water, ethyl alcohol (95%), and diethyl ether. The **C1**
142 obtained was dried in an oven (Model 400/3ND, Nova Etica) at 70.0 °C for 20 min.

143 **2.3. Characterization of C1**

144 **2.3.1. Elemental and spectroscopic analyses**

145 Elemental carbon, hydrogen, and nitrogen analyses of the chitosan and **C1** were
146 performed using an elemental CHNS/O analyzer (Model 2400 Series II, Perkin-Elmer).
147 Before analysis, the materials were dried at 85.0 °C in an oven for 1 h. The analyses were
148 performed in duplicate. Procedures used for characterization of the chitosan and **C1** by
149 Fourier transform infrared (FTIR) and SS ^{13}C NMR spectroscopies were reported by
150 Goncalves et al. (2018).

151 **2.3.2. Surface analyses**

152 The pH of zero charge (pH_{PZC}) of **C1** was determined by the method of Noh and Schwarz
153 (1990). Aqueous 0.10 mol L^{-1} NaNO_3 solutions (150 mL) were prepared and the pH of
154 each solution was adjusted to 3.00, 6.00, or 11.00 by adding drops of aqueous HNO_3
155 (0.1 mol L^{-1}) or NaOH (0.1 mol L^{-1}) solutions. Aliquots of 20.00 mL of each NaNO_3
156 solution at pH 3.00, 6.00, or 11.00 were then added to 125 mL Erlenmeyer flasks to

157 prepare aqueous suspensions of 0.05, 0.1, 0.5, 1.0, and 2.0% ($w v^{-1}$) of **C1**. The flasks
158 were stirred at 130 rpm and 25.0 °C for 24 h in an orbital shaker incubator (Model TE-
159 424, Tecnal). At the end of the experiment, the equilibrium pH of each suspension was
160 measured using a pH meter (Model HI 223, Hanna Instruments). The convergence point
161 of the three curves of equilibrium pH against **C1** concentration ($w v^{-1}$) gave the PZC
162 value.

163 The surfaces of the chitosan and **C1** were analyzed by scanning electron microscopy
164 (SEM) (Model 6510, JEOL). The materials were dried in an oven for 1 h at 80.0 °C,
165 before metallization with a thin layer of carbon graphite (Model JEE-4C, JEOL).

166 The textural properties of **C1** were determined using N_2 adsorption and desorption
167 isotherms obtained using a pore and surface area analyzer (Model Nova 1200e,
168 Quantachrome). **C1** was degassed at 60.0 °C for 24 h before analysis. The specific surface
169 area was determined by the method of Brunauer et al. (1938). The maximum pore
170 diameter was determined by the method of Barrett et al. (1951).

171 **2.4. Adsorption experiments**

172 The **C1** adsorbent was used to adsorb oxyanions of Cr(VI) and Cu(II) from spiked
173 aqueous solutions in batch mono- and bicomponent systems. The adsorption experiments
174 were performed in duplicate, using the experimental conditions described in Table 1. The
175 pH values and buffer solutions were chosen considering the solubility of Cu(II) and
176 Cr(VI) in each buffer solution (Almeida et al., 2016) (see section 4.2.1). The equilibrium
177 pH of each solution was measured using a pH meter (Model HI 223, Hanna Instruments).
178 All flasks (250 mL Erlenmeyers) containing **C1** and solute solutions were stirred in an
179 orbital shaker incubator (Model MA-830, Marconi), followed by a single filtration (C-41

180 (20 μm) filter paper) to separate the spent **C1** adsorbent and the liquid phase. The liquid
181 phases were analyzed by flame atomic absorption spectrophotometry (FAAS) (Model
182 SpectrAA 50B, Varian) ($\lambda_{\text{Cu}} = 324.7 \text{ nm}$, $\lambda_{\text{Cr}} = 425.4 \text{ nm}$) for determination of the Cr(VI)
183 and Cu(II) concentrations (Elias et al., 2019). The FAAS analyses were performed in
184 triplicate.

185 The adsorption capacity (q) of **C1** for oxyanions of Cr(VI) or Cu(II) was determined as
186 follows:

$$187 \quad q / (\text{mmol g}^{-1}) = \frac{(C_0 - C_x)V}{w_{\text{C1}}} \quad (1)$$

188 where, C_0 (mmol L^{-1}) is the initial concentration of oxyanions of Cr(VI) or Cu(II) in the
189 aqueous solution, C_x (mmol L^{-1}) is the concentration of oxyanions of Cr(VI) or Cu(II) at
190 time t or equilibrium, V (L) is the volume of Cr(VI) or Cu(II) aqueous solution, and w_{C1}
191 (g) is the weight of **C1**.

192 **Table 1**

193 **2.4.1. Isothermal titration calorimetry (ITC)**

194 Isothermal titration calorimetry (ITC) experiments were conducted for single adsorption
195 of Cr(VI) (at pH 3.6) and Cu(II) (at pH 5.5), using an Isothermal Titration
196 Nanocalorimeter (Model TAM III, TA Instruments, USA) controlled by dedicated TAM
197 Assistant™ software and equipped with two 4.00 mL reaction cells (sample and
198 reference). Using a Hamilton syringe (500 μL) controlled by a piston pump, stepwise
199 20 μL injections of concentrated buffered aqueous solutions of the metal ions
200 (500.0 mg Cr(VI) L^{-1} or 270.0 mg Cu(II) L^{-1}) were titrated against a mixture of 8.00 mg

201 of **C1** and 2.70 mL of buffer solution in the reaction cell. The reference cell was filled
 202 with the same buffer solution, without the adsorbent. During titration, the time interval
 203 used between consecutive injections was 60 min and a propeller stirrer operating at
 204 180 rpm was used to ensure homogenization of the suspension inside the reaction cell.
 205 Control experiments were performed by *i*) adding the metal ion solution to the buffer
 206 solution in the absence of **C1**, and *ii*) adding the buffer solution to the mixture of
 207 adsorbent and buffer solution, in order to discount the heat effect associated with the
 208 dilutions of the metal ion solutions and **C1** during the adsorption processes. The
 209 measurements were performed at a temperature of 25.0000 ± 0.0001 °C. The solutions
 210 were degassed for 10 min, prior to the titration experiments, in order to avoid bubble
 211 formation in the system. Each titration was performed in duplicate.

212 The change in enthalpy of adsorption for the metal ion adsorption on **C1** ($\Delta_{\text{ads}}H$),
 213 associated with the *i*-th injection in the titration experiment, was calculated as follows:

$$214 \quad \Delta_{\text{ads}}H / (\text{kJ mol}^{-1}) = \frac{q_i - q_{i,\text{dil}}}{n_i} \quad (2)$$

215 where, q_i and $q_{i,\text{dil}}$ (kJ) are the energies absorbed or released in the sample reaction
 216 cell due to the titration processes in the presence of metal ions (Cr(VI) or Cu(II)) and
 217 adsorbent, and in the absence of metal ions or adsorbent, respectively, and n_i (mol) is the
 218 amount of metal ions adsorbed on **C1** during the same injection.

219 **2.4.2. Thermodynamic parameters of adsorption**

220 The approach used for determination of the changes in the standard free energy of
 221 adsorption ($\Delta_{\text{ads}}G^\circ$) for adsorption of Cu(II) and oxyanions of Cr(VI) on **C1** was that
 222 described by Liu (2009), as follows:

223
$$\Delta_{\text{ads}} G^{\circ} / (\text{kJ mol}^{-1}) = -RT \ln \left[\left(\frac{b}{\gamma_e} \right) (1 \text{ mol L}^{-1}) \right] \quad (3)$$

224 where, R is the gas constant ($8.314 \text{ J K}^{-1} \text{ mol}^{-1}$), T (K) is the absolute temperature, and γ_e
 225 is the equilibrium activity coefficient.

226 The value of γ_e can be calculated from the extended Debye Hückel law (Debye and
 227 Hückel, 1923), as follows:

228
$$\log \gamma_e = \frac{-0,509 z^2 \sqrt{I_e}}{1 + \left(\frac{\alpha \sqrt{I_e}}{305} \right)} \quad (4)$$

229 where, z is the charge of the ion, I_e (mol L^{-1}) is the ionic strength at equilibrium, and α
 230 (pm) is the hydrated ion size ($\alpha_{\text{Cu}^{2+}} = 419 \text{ pm}$, $\alpha_{\text{HCrO}_4^-} = 375 \text{ pm}$) (Nightingale, 1959).

231 To obtain the changes in the standard enthalpy of adsorption ($\Delta_{\text{ads}} H^{\circ}$) for adsorption of
 232 Cu(II) and oxyanions of Cr(VI), the $\Delta_{\text{ads}} H$ versus equilibrium concentration of metal ion
 233 (C_e) curves (Figures not shown) were extrapolated to $C_e \rightarrow 0$. The changes in the standard
 234 entropy of adsorption ($\Delta_{\text{ads}} S^{\circ}$) for adsorption of oxyanions of Cr(VI) and Cu(II) were
 235 determined from the following classical thermodynamic relationship:

236
$$\Delta_{\text{ads}} G^{\circ} = \Delta_{\text{ads}} H^{\circ} - T \Delta_{\text{ads}} S^{\circ} \quad (5)$$

237 **2.5. Characterization of C1 loaded with Cu(II) and/or Cr(VI)**

238 C1 loaded with oxyanions of Cr(VI) and/or Cu(II) was analyzed by energy-dispersive X-
 239 ray (EDX) spectroscopy . The materials were dried in an oven at $80.0 \text{ }^{\circ}\text{C}$ for 1 h, followed
 240 by pressing 100 mg portions of the samples denoted **C1-Cu(II)**, **C1-Cr(VI)**, and **C1-**
 241 **Cu(II)-Cr(VI)** in a hydraulic press (Model 181-1110, Pike Technologies) for 1 min, at

242 6 tons, to obtain discs 13 mm in diameter. The discs were metalized with a thin layer of
243 carbon graphite (Model JEE-4C, JEOL) before analysis. The surfaces of the materials
244 were mapped using a scanning electron microscope (Model 6510, JEOL) equipped with
245 an EDX spectrometer (Model X-Max, Oxford Instruments).

246 **2.6. Desorption and reuse of spent adsorbent**

247 The experiments of adsorption and desorption were carried out using the experimental
248 conditions described in Table 2. After desorption, C1 loaded with Cr(VI) or Cu(II) was
249 recovered by single filtration, washed with an excess of ultrapure water, and dried in an
250 oven at 80.0 °C for 6 h (Elias et al., 2019). The other procedures were the same as
251 described in Section 2.4. The desorption efficiency (E_{des}) was determined as follows
252 (Elias et al., 2019):

$$253 \quad E_{des} / \% = \left(\frac{C_e V}{Q_{max} w'_{C1}} \right) \times 100 \quad (6)$$

254 where, Q_{max} (mg g^{-1}) is the maximum adsorption capacity determined for Cr(VI) or
255 Cu(II), and w'_{C1} (g) is the weight of C1 in C1 loaded with Cr(VI) or Cu(II) ($w_{C1,M}$).

256 The value of $w_{C1,M}$ was determined as follows (Elias et al., 2019):

$$257 \quad w'_{C1} / \text{g} = \frac{w_{C1,M} w_{C1}}{\left(\frac{Q_{max} w_{C1}}{1000} \right) + w_{C1}} \quad (7)$$

258 The experiments of re-adsorption were carried out using the experimental conditions
259 described in Table 2. The other procedures were the same as described in Section 2.4.

260 **Table 2**

261 The re-adsorption efficiency ($E_{\text{re-ads}}$) was determined as follows (Elias et al., 2019):

$$262 \quad E_{\text{re-ads}} / \% = \left(\frac{Q_{\text{re-ads,max}}}{Q_{\text{max}}} \right) \times 100 \quad (8)$$

263 where, $Q_{\text{re-ads,max}}$ (mg g^{-1}) is the maximum adsorption capacity of **C1** determined after
264 desorption.

265 The value of $Q_{\text{re-ads,max}}$ was obtained as follows (Elias et al., 2019):

$$266 \quad Q_{\text{re-ads}} / (\text{mg g}^{-1}) = \frac{\left[(w_{\text{C1,M}} - w'_{\text{C1}})(1 - E_{\text{des}}/100) \right] - [(C - C_e)V]}{w'_{\text{C1}}} \quad (9)$$

267 **3. Modeling of the adsorption data**

268 **3.1. Monocomponent adsorption**

269 The data for adsorption of Cu(II) and oxyanions of Cr(VI) on **C1**, as a function of contact
270 time, were modeled using pseudo-first order (Lagergren, 1898) and pseudo-second order
271 models (Ho and McKay, 1999). The mechanism involved in the adsorption of Cu(II) and
272 oxyanions of Cr(VI) on **C1** was investigated using the intraparticle diffusion (IPD)
273 (Weber and Morris, 1963) and Boyd et al. (1947) models. The data for adsorption of
274 oxyanions of Cr(VI) and Cu(II) on **C1**, as a function of initial solute concentration, were
275 modeled using the Langmuir (1918), Sips (1948), and Redlich and Peterson (1959)
276 models.

277 Microcal OriginPro[®] 2015 software was used to perform nonlinear regression (NLR)
278 analysis of the monocomponent adsorption data and to estimate the parameters of the
279 kinetic and equilibrium models. The reduced chi-square (χ^2_{red}) and residual sum of
280 squares (RSS) error functions were used.

281 The equations of the kinetic and equilibrium models as well as the error functions can be
282 found in the Supplementary Material.

283 **3.2. Bicomponent adsorption**

284 The data for the simultaneous adsorption of Cu(II) and oxyanions of Cr(VI) on **C1**, as a
285 function of contact time, were modeled using the model of Corsel et al. (1986). The data
286 for simultaneous adsorption of Cu(II) and oxyanions of Cr(VI) on **C1**, as a function of
287 initial solute concentration, were modeled using the real adsorbed solution theory model
288 (RAST) (Costa et al., 1981; Myers, 1983; Talu and Zwiebel, 1986). The equations of the
289 Corsel and RAST models were those reported by Teodoro et al. (2017; 2018).

290 MATLAB[®] 2010a software (Mathworks Inc., Massachusetts) was used to model the
291 bicomponent adsorption data and estimate the parameters of the kinetic and equilibrium
292 models. The *RSS* error function was used. The computational methods used to solve the
293 equations of the Corsel et al. (1986) and RAST (Costa et al., 1981; Myers, 1983; Talu
294 and Zwiebel, 1986) models were those reported by Teodoro et al. (2017; 2018).

295 **4. Results and discussion**

296 **4.1. Synthesis and characterization of C1**

297 Figure 1 shows the synthesis scheme for preparation of **C1** from the reaction between
298 chitosan and pyridine-2-carbaldehyde. It involved only one step and used ethanol as a
299 green solvent. This synthesis was first reported by our research group (Goncalves et al.,
300 2018). The characterization of the chitosan and **C1** by Fourier transform infrared (FTIR)
301 and SS ¹³C NMR spectroscopies were reported by Goncalves et al. (2018).

302 The C, H, and N elemental analysis of the materials showed that the chitosan and **C1**
303 presented carbon, hydrogen, and nitrogen contents of 41 ± 1 and $49 \pm 1\%$, 7.4 ± 0.2 and
304 $6.2 \pm 0.2\%$, and 7.0 ± 0.2 and $9.0 \pm 0.2\%$, respectively. The contents of carbon and
305 nitrogen increased, while the content of hydrogen decreased, after modification of the
306 chitosan with pyridine-2-carbaldehyde (C = 67.3%, H = 4.71%, N = 13.1%). This
307 indicated that the introduction of pyridine moiety on the biopolymer chain was
308 successfully accomplished.

309 The nitrogen atoms of the imine, pyridine, and remaining amine groups are involved in
310 the adsorption interaction with both species, Cu(II) and Cr(VI), as will be discussed in
311 section 4.2.

312 **Figure 1**

313 The pH of zero charge (pH_{PZC}) of **C1** was determined by the convergence point of three
314 curves of pH (pH_i of 3.00, 6.00, and 11.00) plotted against the **C1** concentration (w v^{-1})
315 (Figure not shown), obtaining a value of 7.6 ± 0.8 . At $\text{pH} < \text{pH}_{\text{PZC}}$, the surface of **C1** is
316 positively charged, due to protonation of the nitrogen atoms of imine, pyridine, and
317 remaining amine groups not modified with pyridine-2-carbaldehyde. Therefore, it is
318 expected that the adsorption of anionic species, such as HCrO_4^- , CrO_4^{2-} , and $\text{Cr}_2\text{O}_7^{2-}$,
319 should be favored at $\text{pH} < \text{pH}_{\text{PZC}}$. Contrarily, the adsorption of cationic species, such as
320 Cu^{2+} and CuOH^+ , should be favored with increase of the pH, with the nitrogen atoms of
321 the imine, pyridine, and remaining amine groups being deprotonated, hence decreasing
322 the positive charge of the **C1** surface, as will be discussed in subsection 4.2.1.

323 Figure 2 presents SEM images of the chitosan and **C1** at $60\times$ and $3,000\times$ magnifications.
324 As can be seen in Figures 2a and 2b ($60\times$ magnification), the physical aspect of the **C1**

325 particles appeared to be unchanged after chemical modification of the chitosan with
326 pyridine-2-carbaldehyde. However, the SEM images at 3,000× magnification (Figures 2b
327 and 2d) revealed that the surface texture of **C1** was significantly different from the
328 chitosan surface texture. The **C1** surface was rougher than the chitosan surface, indicating
329 that it had been chemically modified by the grafting of pyridine-2-carbaldehyde
330 molecules. In addition, the **C1** surface presented some cracks, indicating that the **C1**
331 particles swelled after chemical modification with pyridine-2-carbaldehyde.

332 **Figure 2**

333 The specific surface areas of the chitosan and **C1** were $19 \text{ m}^2 \text{ g}^{-1}$, the average diameter of
334 micropores were 20 \AA while the maximum pore diameters were 444 and 595 \AA ,
335 respectively. Therefore, chitosan and **C1** also present meso and macropores, respectively.
336 These results showed that the chemical modification of chitosan with pyridine-2-
337 carbaldehyde did not change the specific surface area of **C1**, compared to the non-
338 modified chitosan. Contrarily, the maximum pore diameter increased after modification
339 of the chitosan. To know the distribution of micro, meso, and macropores is important for
340 the evaluation of ion diffusion and ion transportation process from the solution bulk to
341 porous structure of the **C1** adsorbent (subsections 4.2.2 and 4.3.2).

342 The average particle size was 0.5 mm and no disintegration or swelling of the **C1** particles
343 was observed during the adsorption experiments described in the following sections.

344 **4.2. Monocomponent adsorption of Cu(II) and oxyanions of Cr(VI) on C1**

345 **4.2.1. Adsorption of Cu(II) and oxyanions of Cr(VI) on C1, as a function of solution** 346 **pH**

347 Figure 3a shows the changes in equilibrium adsorption capacity (q_e), as a function of
348 solution pH, for the adsorption of Cu(II) and oxyanions of Cr(VI) on C1.

349 **Figure 3**

350 At low pH ($\text{pH} < 3.5$), the nitrogen atoms of imine, pyridine, and remaining amine groups
351 on C1 ($\text{pH}_{\text{PZC}} = 7.6 \pm 0.8$) are protonated ($\text{p}K_{\text{a,imine}} = 5-7$, $\text{p}K_{\text{a,pyridine}} = 5.2$), so Cu(II)
352 adsorption was not observed (Figure 3a). From pH 4.0, the value of q_e for Cu(II)
353 adsorption augmented with increasing solution pH up to pH 5.5, because the nitrogen
354 atoms of the imine, pyridine, and remaining amine groups became deprotonated as the
355 solution pH increased. This enabled interaction between the lone electron pairs of
356 nitrogen atoms and the Cu(II) ions (Figure 1b, C1-Cu²⁺). The adsorption of Cu(II) was
357 not evaluated at pH higher than 5.5, due to the formation of hydrolyzed Cu(II) species,
358 such as Cu(OH)⁺ and Cu(OH)₂ (Eqs. (17)-(20)).

359 Cr(VI) can form various species in aqueous solution, such as H₂CrO₄, HCrO₄⁻, CrO₄²⁻,
360 and Cr₂O₇²⁻, depending on the total Cr(VI) concentration, pH, and ionic strength (I) of the
361 solution. Supplementary Figure 1 presents graphs of the fraction of Cr(VI) species, as a
362 function of solution pH from 0 to 10, for total Cr(VI) concentrations of 0.77 and
363 3.85 mmol L⁻¹. At a total Cr(VI) concentration of 0.77 mmol L⁻¹ ($I = 0.05$ mol L⁻¹), the
364 HCrO₄⁻ species (fraction of ~0.9) predominates over the Cr₂O₇²⁻ species (fraction of ~0.1)
365 in the pH range from 1 to 5. At pH 1.0, the HCrO₄⁻ species (fraction of ~0.85) still
366 predominates over Cr₂O₇²⁻ (fraction of ~0.10) and H₂CrO₄ (fraction of ~0.05). Contrarily,
367 as the solution pH increased from 5 to 8, the CrO₄²⁻ fraction increased from ~0.10 to 1.0,
368 predominating over HCrO₄⁻ (which decreased from ~0.9 to 0) and Cr₂O₇²⁻ (which
369 decreased from ~0.1 to 0).

370 At low pH ($\text{pH} < 4$), the nitrogen atoms of the imine, pyridine, and remaining amine
371 groups on **C1** are protonated, resulting in strong electrostatic attraction between the
372 positively charged **C1** surface and the negatively charged oxyanions of Cr(VI) (HCrO_4^-
373 and $\text{Cr}_2\text{O}_7^{2-}$) (Figure 1b). This explains the higher value of q_e for Cr(VI) adsorption at pH
374 3.5 (Figure 3a). At pH lower than 3.5, competition between HCrO_4^- and $\text{Cr}_2\text{O}_7^{2-}$ for **C1**
375 surface sites, together with repulsive lateral interactions between adsorbed Cr(VI)
376 species, could have contributed to decreasing the value of q_e for Cr(VI) adsorption.
377 Anions with higher charge density and multivalent anions are more strongly adsorbed by
378 electrostatic attraction (Lv et al., 2006). The charge/radius (Z/r) ratio of $\text{Cr}_2\text{O}_7^{2-}$ ($2/2.92$)
379 (Haynes et al., 2014) is higher than that of HCrO_4^- ($1/2.42$) (Motzer, 2004), suggesting
380 that $\text{Cr}_2\text{O}_7^{2-}$ is preferentially adsorbed on the **C1** surface in the pH range from 2 to 4, in
381 the presence of HCrO_4^- . As the solution pH was increased from 3.5 to 8, the nitrogen
382 atoms of the imine, pyridine, and remaining amine groups on **C1** were gradually
383 deprotonated, hence decreasing the electrostatic attraction between the **C1** surface and
384 the oxyanions of Cr(VI) (HCrO_4^- , CrO_4^{2-} , and $\text{Cr}_2\text{O}_7^{2-}$). At pH higher than 7
385 ($\text{pH}_{\text{PZC}} = 7.6 \pm 0.8$), the adsorption of Cr(VI) species (HCrO_4^- and CrO_4^{2-}) was close to
386 zero, because the **C1** surface was almost deprotonated.

387 Therefore, the subsequent studies of adsorption of Cr(VI) and Cu(II) species on **C1** were
388 carried out at the pH values of maximum adsorption. As pointed out by Wan Ngah et al.
389 (2011), the solubility and swelling properties of raw chitosan are the main existing
390 bottlenecks for its application as an adsorbent. On the other hand, **C1** stability (solubility
391 and swelling) was not affected in the pH range studied. This is an advantage of **C1** in
392 comparison to raw chitosan, which was soluble in the acidic pH values tested in the
393 present study.

394 **4.2.2. Adsorption of Cu(II) and oxyanions of Cr(VI) on C1, as a function of contact**
395 **time**

396 Figures 3b and 3c show the change in adsorption capacity (q_t), as a function of contact
397 time, for the adsorption of Cu(II) and oxyanions of Cr(VI) on C1, respectively. In Table
398 3 are presented the kinetic parameters obtained by modeling the adsorption of Cu(II) and
399 oxyanions of Cr(VI) on C1, using the PFO and PSO models, as well as the Boyd and
400 intraparticle diffusion models. The PSO kinetic model provided the best description of
401 the adsorption of oxyanions of Cr(VI) (HCrO_4^- and $\text{Cr}_2\text{O}_7^{2-}$) and Cu(II) on C1. The values
402 of the R^2 and χ^2_{red} error functions were higher and lower, respectively, comparing the PSO
403 model with the PFO model. In addition, the values of $q_{e,\text{est}}$ (estimated equilibrium
404 adsorption capacity) calculated using the PSO model were closer to the $q_{e,\text{exp}}$ values
405 (experimental equilibrium adsorption capacity) for the adsorption of oxyanions of Cr(VI)
406 and Cu(II) on C1. As can be seen in Figures 3b and 3c, q_e was reached at 240 and 360 min
407 for the adsorption of Cu(II) and oxyanions of Cr(VI) on C1, respectively.

408 According to Plazinski et al. (2013), the PSO model can be interpreted in terms of surface
409 reaction models or in terms of the intraparticle diffusion model. The first consider that
410 the transfer of adsorbate throughout the solution/solid interface is the slowest step in the
411 entire adsorption process. The second considers that the overall adsorption rate is
412 controlled by the rate of adsorbate diffusion within the pores of the adsorbent (Plazinski
413 et al., 2013). On the other hand, the PFO model can be interpreted considering that the
414 adsorption kinetics is determined by the rate of diffusional transport of a solute (Plazinski
415 et al., 2009) as suggested by Boyd et al. (1947). This model is a film diffusion model
416 represented by an equation with the same analytical form as the PFO model

417 **Table 3**

418 The mechanisms of adsorption of Cu(II) and oxyanions of Cr(VI) on **C1** were evaluated
419 from the Boyd and intraparticle diffusion plots. These graphs are available in the
420 Supplementary Material (Supplementary Figures 2 and 3). The intraparticle diffusion
421 plots for the adsorption of oxyanions of Cr(VI) and Cu(II) on **C1** showed two and three
422 stages, respectively. The straight lines representing the first stages did not intersect the
423 origin ($C \neq 0$), indicating that the adsorption was influenced by the diffusion of the ions
424 through the thin solvent layer surrounding the **C1** particles. Two stages were observed
425 for Cu(II) adsorption, reflecting a shift from film diffusion (first stage) to intraparticle
426 diffusion (second stage), after 10 min.

427 The Boyd plots for adsorption of Cu(II) and oxyanions of Cr(VI) on **C1** were linear for
428 $f < 0.85$ and presented intercept values close to zero, suggesting that external mass
429 transfer of solute through the thin solvent layer affected the adsorption of both ions on
430 **C1**. The effective diffusion coefficients (D_i) (Table 3) for adsorption of Cu(II) and
431 oxyanions of Cr(VI) on **C1** were of the same order of magnitude ($10^{-11} \text{ m}^2 \text{ min}^{-1}$), with
432 Cr(VI) ions diffusing 4-fold faster than Cu(II) ions from the bulk solution to the **C1**
433 external surface. Although Cr(VI) ions are heavier than Cu(II) ions, the diffusion of
434 Cr(VI) ions was faster than the diffusion of Cu(II) ions. This behavior may be explained
435 by the larger hydrated ion size (α) of the Cu(II) ion ($\alpha_{\text{Cu}^{2+}} = 419 \text{ pm}$, $\alpha_{\text{HCrO}_4^-} = 375 \text{ pm}$,
436 (Nightingale, 1959).

437 **4.2.3. Adsorption of Cu(II) and oxyanions of Cr(VI) on C1, as a function of initial** 438 **solute concentration**

439 Adsorption isotherms are of fundamental importance for providing relevant information
440 about adsorption systems. The isotherm represents the adsorption behavior of a solute on

441 an adsorbent, according to increasing solute concentration, at constant temperature and
442 pH. The adsorption isotherm is also used to estimate the maximum adsorption capacity
443 (Q_{\max}) of a solute on an adsorbent. Various isotherm models have been proposed for
444 fitting the equilibrium data in the form of a plot of q_e against C_e . Some model equations
445 have two or more adjustable parameters, such as those of the Langmuir (1918), Sips
446 (1948), and Redlich and Peterson (1959) (R-P) models.

447 Figures 3d and 3e present plots of q_e against C_e for the adsorption of Cu(II) and oxyanions
448 of Cr(VI) on **C1**, respectively. The isotherm models that best described the adsorption of
449 Cu(II) on **C1** were the Langmuir and Sips models. The values of the adjustable parameters
450 obtained by modeling the equilibrium data using the Langmuir, R-P, and Sips models are
451 presented in Table 3. These models presented higher R^2 values and lower χ^2_{red} values
452 (Table 3). The parameter n of the Sips isotherm reflects the heterogeneity of an adsorption
453 system. The value of n for Cu(II) adsorption on **C1** was close to unity, suggesting that the
454 Sips isotherm model could be reduced to the Langmuir isotherm model. The Langmuir
455 model is based on premises that are not valid for the system investigated in the present
456 study. Nevertheless, Langmuir model is as a suitable mathematical descriptor to estimate
457 the maximum adsorption capacity. Aspects related to the heterogeneity of the adsorption
458 sites will be discussed in more in-depth in thermodynamic studies (subsection 4.2.4).

459 The Sips model provided the best description of the adsorption of oxyanions of Cr(VI)
460 on **C1**, with higher R^2 values and lower χ^2_{red} values (Table 3). Since the value of n was
461 much smaller than unity, the Sips isotherm model could not be reduced to the Langmuir
462 isotherm model for Cr(VI) adsorption.

463 Considering that Cu(II) and Cr(VI) were adsorbed on the same adsorbent (**C1**), the results
464 suggested that: 1) Cu(II) adsorption occurred on homogeneous sites, and 2) Cr(VI)

465 adsorption did not occur on homogeneous sites. Hypothesis 1 is compatible with the
466 formation of inner-sphere complexes, which requires a particular electronic configuration
467 of the adsorbent (specific sites) and the adsorbate. Hypothesis 2 is compatible with the
468 adsorption of different Cr(VI) species.

469 The value of Q_{\max} for adsorption of oxyanions of Cr(VI) on **C1** was 2-fold higher than
470 the value of Q_{\max} for adsorption of Cu(II) on **C1**. A possible explanation for this result is
471 that adsorption of Cu(II) on the **C1** surface may have been occurred by the formation of
472 bidentate inner-sphere complexes with nitrogen atoms of imine and pyridine groups
473 (Figure 1b) (Brown et al., 1995; Sposito, 2008). On the other hand, within the Cr(VI)
474 concentration range studied (0.15-7 mmol L⁻¹), HCrO₄⁻ species prevailed over Cr₂O₇²⁻
475 species. This suggests the possible formation of outer-sphere complexes between two
476 HCrO₄⁻ species and positively charged nitrogen atoms of imine and pyridine groups
477 (Figure 1b) (Brown et al., 1995; Sposito, 2008).

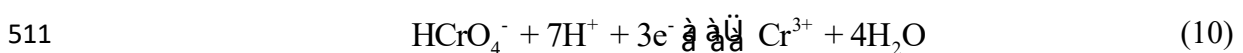
478 **C1** presented a higher Q_{\max} than other bioadsorbents reported in the literature (Chen et
479 al., 2016; Dong et al., 2010). For example, Chen et al. (2016) used carbonized crofton
480 weed (*Eupatorium adenophorum*) and Dong et al. (2010) used a crosslinked amino starch
481 for Cu(II) and Cr(VI) adsorption from aqueous solutions. Chen et al. (2016) reported Q_{\max}
482 values of 0.19 and 0.44 mmol g⁻¹ for adsorption of Cr(VI) and Cu(II), respectively (pH
483 5.0, 25 °C). The crosslinked amino starch reported by Dong et al. (2010) was produced
484 by chemical modification of dialdehyde starch with ethylenediamine and presented Q_{\max}
485 values of 0.13 and 0.23 mmol g⁻¹ for adsorption of Cu(II) and Cr(VI), respectively (pH
486 3.0-5.0, 30 °C) (Dong et al., 2010). In a previous study, Almeida et al. (2016) reported
487 the synthesis of an efficient adsorbent by quaternization of the amine group of chitosan
488 and esterification of -OH groups with EDTA dianhydride. This chitosan derivative

489 showed Q_{\max} values of 0.698 and 1.91 mmol g⁻¹ for adsorption of Cu(II) (pH 4.5, 25 °C)
490 and Cr(VI) (pH 2.0, 25 °C), respectively. Table 4 shows different adsorbent materials that
491 have been applied for the removal of both Cu(II) and Cr(VI) from aqueous solution.

492 The Langmuir constant, b , reflected the affinity of the C1 adsorption surface sites for
493 oxyanions of Cr(VI) or Cu(II). The value of b was much higher for adsorption of Cu(II)
494 than for adsorption of Cr(VI), which was in agreement with the hypotheses raised.

495 As discussed previously, Cr(VI) can form various species in aqueous solution
496 (Supplementary Figure 1), depending on the chemical conditions of the solution. The
497 speciation of Cr also depends on the redox conditions (solution Eh). The reduction of
498 Cr(VI) to Cr(III) can occur under specific conditions that depend on the presence of light
499 irradiation or substances that can promote reduction. For example, Fida et al. (2015)
500 employed a bifunctional Ti-Fe kaolinite composite with adsorption and photocatalytic
501 properties to remove Cr(VI) from water. According to Fida et al. (2015), the reduction of
502 Cr(VI) to Cr(III) was promoted by visible light irradiation, associated with TiO₂ and the
503 Fe(III)/Fe(II) redox cycle. Wang et al. (2020) reported the use of nanoscale Fe⁰ with a
504 cellulose hydrogel coating for Cr(VI) reduction and adsorption. According to Wang et al.
505 (2020), the cellulose hydrogel firstly promoted physical adsorption, transferring Cr(VI)
506 from the solution to the Fe⁰ particles, where it was immobilized by electrostatic attraction.
507 The Cr(VI) was then reduced to Cr(III) by Fe⁰ from the adsorbent.

508 Nevertheless, in the present study, the results did not indicate the occurrence of reduction
509 of Cr(VI) to Cr(III). This reduction is also strongly dependent on the solution pH,
510 according to the following chemical equation:



512 Therefore, the reduction of Cr(VI) to Cr(III) consumes H_3O^+ , consequently increasing the
513 solution pH. However, there was no increase of the solution pH in any of the adsorption
514 studies. Furthermore, the absence of change in the behavior of the curves of adsorption
515 capacity for Cr(VI) as a function of contact time (Figure 3c) and equilibrium solute
516 concentration (Figure 3e) provided additional evidence that there was no reduction of
517 Cr(VI) to Cr(III). It should also be noted that the formation of Cr(III) would be observed
518 by the appearance of a green coloration in the solution and on the adsorbent surface after
519 adsorption. This was not observed. Therefore, there was no experimental evidence of the
520 reduction of Cr(VI) to Cr(III), under the experimental conditions studied.

521 Thermodynamic analysis (subsection 4.2.4) provided further elucidation of the nature of
522 the interactions involved in the Cr(VI) or Cu(II) adsorption on **C1**. For example, the
523 values of $\Delta_{ads}H$ plotted against q_e , for the adsorption of Cr(VI) on **C1** (Figure 4), were
524 much lower than the values expected for oxidation-reduction processes. Additionally, the
525 energies were of the same order of magnitude as those obtained for Cu(II) adsorption.
526 Therefore, these results support the hypothesis that there was no Cr(VI) reduction.

527 **4.2.4. Adsorption thermodynamics analysis**

528 ITC measurements were performed in order to obtain more information about the nature
529 of the interactions governing the adsorption of Cu(II) and oxyanions of Cr(VI) on **C1**.
530 ITC is a sensitive technique that provides the amount of energy released or absorbed in
531 an isothermal thermodynamic process. Figure 4 shows the curves of $\Delta_{ads}H$ plotted against
532 q_e , for the adsorption of oxyanions of Cr(VI) and Cu(II) on **C1** at 25 °C.

533 **Figure 4**

534 The adsorption processes of oxyanions of Cr(VI) and Cu(II) on **C1** were exothermic over
 535 the range of surface coverage of **C1** studied, changing from -30.3 ± 0.2 to -
 536 15.6 ± 0.1 kJ mol⁻¹ for Cr(VI) species and from -30.6 ± 0.6 to -10.8 ± 0.9 kJ mol⁻¹ for
 537 Cu(II). The $\Delta_{\text{ads}}H$ values were more negative for oxyanions of Cr(VI) than for Cu(II),
 538 indicating that the balance of the interactions involving the adsorption of Cr(VI) species
 539 was more favorable. As q_e increased, the adsorptions of oxyanions of Cr(VI) and Cu(II)
 540 became less enthalpically favorable, suggesting the existence of heterogeneous
 541 adsorption processes in both cases. Additionally, the slopes of the $\Delta_{\text{ads}}H$ versus q_e curves
 542 ($d\Delta_{\text{ads}}H/dq_e$) were very different, indicating different interactions for the adsorption of
 543 oxyanions of Cr(VI) and Cu(II) on **C1**.

544 In order to better understand these results, the $\Delta_{\text{ads}}H$ value observed for each q_e value
 545 could be considered as the sum of the following independent terms:

$$546 \quad \Delta_{\text{ads}}H = \Delta_{\text{ads}}H^{\text{C1-M}} + \Delta_{\text{ads}}H^{\text{des}} + \Delta_{\text{ads}}H^{\text{M-M}} \quad (11)$$

547 where, $\Delta_{\text{ads}}H^{\text{C1-M}}$ is the change in the enthalpy of adsorption (negative) due to the
 548 formation of interactions between the metal ion species and the adsorption sites on **C1**;
 549 $\Delta_{\text{ads}}H^{\text{des}}$ is the change in the enthalpy of adsorption (positive or negative) associated with
 550 the desolvation processes of the metal ion species and the adsorbent surface sites for the
 551 formation of inner/outer-sphere complexes; and $\Delta_{\text{ads}}H^{\text{M-M}}$ is the change in the enthalpy
 552 of adsorption (positive or negative) associated with the absorption and release of energy
 553 when interactions between the metal ion species are formed on the **C1** surface and
 554 disrupted in the solution, respectively, during the adsorption process.

555 At the first adsorbed amount value in the $\Delta_{\text{ads}}H$ versus q_e curves, when the surface
 556 coverage and the concentration of the metal ion species in the bulk solvent were low, the

557 contribution of the $\Delta_{\text{ads}}H^{M-M}$ term was negligible and the $\Delta_{\text{ads}}H$ values were determined
558 by the magnitudes of the $\Delta_{\text{ads}}H^{C1-M}$ and $\Delta_{\text{ads}}H^{\text{des}}$ terms. Since the process was exothermic
559 under this condition, there should be an important contribution of the interactions between
560 the **C1** adsorption sites and oxyanions of Cr(VI) or Cu(II), which released energy, because
561 the desolvation of the functional groups containing nitrogen atoms and the metal ion
562 species required a high amount of energy (Marcus, 1987b). Part of the desolvation energy
563 was due to the dehydration of the metal ion species, with the displacement of water
564 molecules from the solvation shells of the ions to bulk solution. Since Cu(II) could form
565 inner-sphere complexes with the lone electron pairs of the nitrogen atoms on **C1**, the
566 displacement of water molecules from the first solvation shell of these ions should result
567 in a more endothermic $\Delta_{\text{ads}}H^{\text{des}}$ term for this metal ion, compared to the oxyanions of
568 Cr(VI), which could form outer-sphere complexes. This could explain the less negative
569 values of $\Delta_{\text{ads}}H$ for Cu(II) adsorption.

570 As q_e increased, repulsive lateral interactions between the adsorbed ions increased, due
571 to the decreased distance between the adsorbed metal ion species on the **C1** surface,
572 contributing to positive values for $\Delta_{\text{ads}}H^{M-M}$. At the same time, due to the heterogeneity
573 of the adsorbent surface, the magnitudes of both $\Delta_{\text{ads}}H^{\text{des}}$ and $\Delta_{\text{ads}}H^{C1-M}$ were changed,
574 contributing to the increase of $\Delta_{\text{ads}}H$ (less negative values).

575 The **C1** adsorbent possessed different functional groups containing nitrogen atoms
576 (imine, pyridine, and remaining amine groups), which implied the existence of adsorption
577 sites with different adsorption molar enthalpy changes. When the surface coverage
578 increased, adsorption sites with lower adsorption molar enthalpy change were occupied
579 by the ions, increasing the $\Delta_{\text{ads}}H^{C1-M}$ value. Additionally, for the pH range evaluated,
580 especially pH 5.5, some of the functional groups on **C1** were partially protonated ($pK_{a,\text{imine}}$

581 = 5-7, $pK_{a,\text{pyridine}} = 5.2$), which provided a wider variety of functional groups for Cu(II)
582 adsorption. Greater heterogeneity of the **C1** surface for Cu(II) adsorption could explain
583 the higher slope of the $\Delta_{\text{ads}}H$ versus q_e curve for the adsorption of this species.

584 In order to evaluate the thermodynamically driven forces for the adsorption of the metal
585 ion species and corroborate the hypothesis mentioned previously, adsorption
586 thermodynamic parameters were obtained under the standard conditions. The values of
587 $\Delta_{\text{ads}}G^\circ$, $\Delta_{\text{ads}}H^\circ$, and $T\Delta_{\text{ads}}S^\circ$ were -26 ± 2 , -33.0 ± 0.8 , and -7 ± 3 kJ mol⁻¹ for Cu(II) and
588 -21 ± 3 , -35.2 ± 0.2 , and -14 ± 3 kJ mol⁻¹ for Cr(VI), respectively. For Cr(VI), it was
589 considered that HCrO_4^- predominated over $\text{Cr}_2\text{O}_7^{2-}$ ($\alpha = 375$ pm, $\gamma_e = 0.415$, and
590 $\Delta_{\text{ads}}G^\circ = -23 \pm 3$ kJ mol⁻¹, at pH 3.6), with an equilibrium concentration of 3.85 mmol L⁻¹
591 and I_e of 0.06 mol L⁻¹ (Supplementary Figure 1b). The values of $\Delta_{\text{ads}}G^\circ$ obtained in the
592 present study were similar to those reported by Almeida et al. (2016) for Cr(VI) ($-$
593 21 ± 1 kJ mol⁻¹) and Cu(II) (-20 ± 6 kJ mol⁻¹).

594 The change in the free energy of adsorption ($\Delta_{\text{ads}}G^\circ$) was negative for adsorption of Cu(II)
595 and oxyanions of Cr(VI) on **C1**, indicating that under the standard conditions, the transfer
596 processes of both species from the bulk solution to the adsorbent surface were favorable
597 and that oxyanions of Cr(VI) and Cu(II) were concentrated on the **C1** adsorbent surface
598 under the equilibrium condition. The $\Delta_{\text{ads}}H^\circ$ and $\Delta_{\text{ads}}S^\circ$ parameters were negative,
599 indicating that the adsorption was enthalpically driven and entropically unfavorable.
600 However, the entropy loss for the adsorption of oxyanions of Cr(VI) was much higher.
601 The change in the standard entropy of adsorption is mainly due to the rotational,
602 translational, and electrostatic contributions from the free metal ions in the bulk solution
603 and the ion pairs formed on the **C1** adsorbent surface (Marcus, 1987a). The main change
604 in the entropy of the system arises from *i*) decrease of the degrees of freedom of the metal

605 ion species, due to their transfer from the bulk solution to the **C1** surface, and *ii*) increase
 606 of the degrees of freedom of water molecules when they are released from the solvation
 607 shells of the ions and the **C1** surface sites to the bulk solution, because of the formation
 608 of inner/outer-sphere complexes. As the $\Delta_{\text{ads}}S^\circ$ value was negative, the entropy gain
 609 related to the process of release of water molecules did not exceed the entropy loss related
 610 to the process of formation of ion pairs, i.e. inner/outer-sphere complexes on the **C1**
 611 adsorbent surface. The lower loss of entropy for Cu(II) adsorption was probably due to
 612 the release of a greater number of water molecules more strongly bound to the metal ion
 613 solvation shell, for the formation of inner-sphere complexes with the **C1** adsorption sites,
 614 as well as the difference associated with the contribution of the rotational entropy of this
 615 type of complex (Marcus, 1987a).

616 **4.3. Bicomponent adsorption of Cu(II) and oxyanions of Cr(VI) on C1**

617 The presence of both oxyanions of Cr(VI) and Cu(II) cations in aqueous solution may
 618 lead to the formation of CuCrO_4 precipitate. Therefore, the solubility (S , mmol L^{-1}) of
 619 CuCrO_4 was calculated using Eq. (12).

$$620 \quad S = (K_{\text{sp}} \alpha \beta)^{1/2} \quad (12)$$

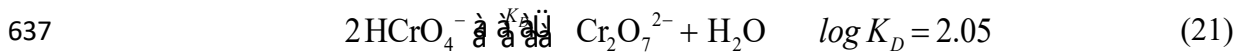
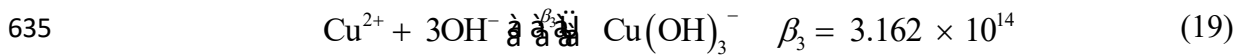
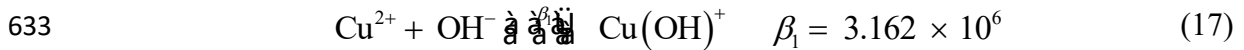
621 with,

$$622 \quad \alpha = \frac{[\text{H}_3\text{O}^+]^2}{K_{\text{a}2}K_{\text{a}1}} + \frac{[\text{H}_3\text{O}^+]}{K_{\text{a}2}} + 1 \quad (13)$$

$$623 \quad \beta = 1 + \beta_1[\text{HO}^-] + \beta_2[\text{HO}^-]^2 + \beta_3[\text{HO}^-]^3 + \beta_4[\text{HO}^-]^4 \quad (14)$$

624 where, K_{sp} is the solubility product constant of CuCrO_4 ($K_{\text{sp}} = 3.6 \times 10^{-6}$ (Harris, 2010)),
 625 $K_{\text{a}1}$ and $K_{\text{a}2}$ are the ionization constants of acidic species of Cr(VI) (Eqs. (15)-(16)), and

626 $\beta_1, \beta_2, \beta_3,$ and β_4 are the formation constants of Cu(II)-hydroxy complexes (Eqs. (17)-(20)
 627). Here, the dimerization of chromate to dichromate (Eq. (21)) was not considered,
 628 because all the dichromate salts are soluble in water. Bicomponent adsorption studies
 629 (presented in the next sections) were performed using pH values and concentrations of
 630 Cu(II) and oxyanions of Cr(VI) at which CuCrO_4 precipitation does not occur.



638 **4.3.1. Simultaneous adsorption of Cu(II) and oxyanions of Cr(VI) on C1, as a**
 639 **function of solution pH**

640 Figure 5a presents a graph of q_e plotted against solution pH (from 3.6 to 5.5) for the
 641 simultaneous adsorption of Cu(II) and oxyanions of Cr(VI) on C1. If the value of
 642 $q_{\text{multi}}/q_{\text{mono}}$ is < 1 , the adsorption of a solute i is disfavored by the presence of a solute j .
 643 In contrast, when the value of $q_{\text{multi}}/q_{\text{mono}}$ is > 1 , the adsorption of a solute i is favored by
 644 the presence of a solute j . When the value of $q_{\text{multi}}/q_{\text{mono}}$ is 1, the presence of a solute i

645 does not affect the adsorption of a solute j . The values of $q_{\text{multi}}/q_{\text{mono}}$ (0.6-0.8) for Cr(VI)
646 adsorption from pH 3.6 to 4.5 were lower than unity, showing that the presence of Cu(II)
647 disfavored the adsorption of Cr(VI) on **C1**. However, from pH 5.0 to 5.5, where the CrO_4^{2-}
648 concentration begins to increase, the presence of Cu(II) favored Cr(VI) adsorption
649 ($q_{\text{multi}}/q_{\text{mono}} = 1.5$, at pH 5.0). This was indicative of cooperative adsorption between
650 oxyanions of Cr(VI) and Cu(II). The values of $q_{\text{multi}}/q_{\text{mono}}$ (17.9-1.2) for Cu(II) adsorption
651 from pH 3.6 to 4.5 were higher than unity, showing that the presence of oxyanions of
652 Cr(VI) favored Cu(II) adsorption. This also indicated cooperative adsorption between
653 Cu(II) and oxyanions of Cr(VI). However, from pH 5.0 to 5.5, the presence of oxyanions
654 of Cr(VI) disfavored the Cu(II) adsorption ($q_{\text{multi}}/q_{\text{mono}} = 0.5$, at pH 5.0).

655 The Cu(II) ions were probably adsorbed on the **C1** surface by the formation of inner-
656 sphere complexes, while oxyanions of Cr(VI) were adsorbed on the **C1** surface by the
657 formation of outer-sphere complexes. These two types of adsorption, known as localized
658 (specific, (Cu(II)) adsorption and delocalized (nonspecific, oxyanions of Cr(VI))
659 adsorption, allowed the formation of a Stern layer on the **C1** surface. As the solvated
660 Cu(II) ions did not form complexes with oxyanions of Cr(VI) adsorbed on the **C1** surface,
661 and vice-versa, they approached the **C1** surface and were attached by delocalized
662 (nonspecific) adsorption (Sposito, 2008). Therefore, a hypothesis for the cooperative
663 adsorption between oxyanions of Cr(VI) and Cu(II) ions was the formation of a diffuse
664 ion swarm, involving ions fully dissociated from the **C1** surface functional groups and
665 free to approach nearby adsorbed species on the **C1** surface (Sposito, 2008). This type of
666 interaction only involves electrostatic bonding.

667 The highest simultaneous adsorption capacity (1.96 mmol g^{-1}) for oxyanions of Cr(VI)
668 and Cu(II) was observed at pH 4.5. Therefore, a pH of 4.5 was considered as the optimum
669 for simultaneous adsorption of both solutes on C1.

670 **Figure 5**

671 **4.3.2. Simultaneous adsorption of Cu(II) and oxyanions of Cr(VI) on C1, as a**
672 **function of contact time**

673 The competitive model of Corsel et al. (1986) was adopted to describe the
674 multicomponent adsorption kinetics. Although the PFO and PSO models can be used to
675 model the individual adsorption kinetic curves in a competitive adsorption of metal ions
676 in aqueous solution, these models cannot describe the interactions between ions. On the
677 contrary, the competitive adsorption model developed by Corsel et al. (1986) can be used
678 to model both adsorption kinetic curves simultaneously, allowing the understanding of
679 the interactions between ions, i.e., how the adsorption of a species i affects the adsorption
680 of a species j and vice versa. This model includes the intrinsic adsorption ($k(I)^{\text{app}_{\text{on}}}$) and
681 desorption ($k(I)^{\text{app}_{\text{off}}}$) rate constants, which employ the adsorption capacity normalized
682 by the specific area of the adsorbent (I). The model considers the deviations from ideal
683 behavior assumed by the Langmuir model. The kinetic model of Corsel et al. (1986),
684 which is based on first-order reaction kinetics, employs a generalized diffusion equation.
685 It enables inclusion of the effect of the surrounding bulk medium (unstirred layer)
686 (Teodoro et al., 2017).

687 In previous studies, the Corsel model (Corsel et al., 1986) was employed to model the
688 kinetics of the competitive adsorption of metal cations (Teodoro et al., 2017) and cationic
689 dyes (Fideles et al., 2019) on lignocellulosic materials. Teodoro et al. (2017) studied the

690 adsorption of the binary systems Cu(II)/Co(II), Cu(II)/Ni(II), and Co(II)/Ni(II) on a
691 carboxylated cellulose derivative. Fidelis et al. (2019) studied the bicomponent
692 adsorption of auramine-O and safranin-T on trimellitated sugarcane bagasse. In both
693 studies, it was concluded that the Corsel model was more suitable for describing
694 bicomponent adsorption systems, because it takes into consideration the competition
695 between the adsorbate species for the adsorbent sites.

696 The kinetic parameters estimated by the Corsel et al. (1986) are presented in Table 5.
697 Figure 5b presents a graph of $I(t)$ plotted against t . The equilibrium time ($t_{e,multi}$) for
698 simultaneous adsorption of Cu(II) and oxyanions of Cr(VI) was 180 min, while the
699 equilibrium times ($t_{e,mono}$) for monocomponent adsorption of Cu(II) and oxyanions of
700 Cr(VI) were 240 and 360 min, respectively. This suggested that the presence of Cu(II)
701 decreased the equilibrium time for adsorption of oxyanions of Cr(VI), and vice-versa.
702 This result could be an indication of cooperative adsorption between Cr(VI) and Cu(II),
703 due to electrostatic interaction between these ions. A possible cooperative effect in the
704 adsorption of Cu(II) and Cr(VI) was also reported by Shen et al. (2012), who studied the
705 use of amino-functionalized nano-Fe₃O₄ magnetic polymers for adsorption of Cu(II)
706 (100 mg L⁻¹) and Cr(VI) (200 mg L⁻¹) co-existing in a water system. It was concluded
707 that there might be cooperative adsorption processes, although competitive adsorption
708 was observed at higher concentrations of Cr(VI) and Cu(II).

709 The association constant (K) is related to the affinity of a solute i for the surface
710 adsorption sites of an adsorbent, in the presence of a solute j . The value of K is calculated
711 by the ratio of the adsorption (k_{+1}) and desorption (k_{-1}) rate constants, k_{+1}/k_{-1} (Teodoro et
712 al., 2017). The value of K was higher for Cr(VI) adsorption than for Cu(II) adsorption,
713 indicating that the affinity of the C1 surface sites for oxyanions of Cr(VI), in the presence

714 of Cu(II), was higher than the affinity of the C1 surface sites for Cu(II) ions, in the
715 presence of oxyanions of Cr(VI). This behavior was not expected, because the value of b
716 for monocomponent adsorption of Cu(II) ($17 \pm 1 \text{ L mmol}^{-1}$) was much higher than that
717 for monocomponent adsorption of oxyanions of Cr(VI) ($3.8 \pm 0.5 \text{ L mmol}^{-1}$). This
718 confirmed the non-ideal behavior of the adsorption of Cu(II) ions in the presence of
719 oxyanions of Cr(VI), and vice-versa.

720 The interaction constants α and β for the adsorption and desorption of a solute at an
721 adsorbent, respectively, provide useful information about lateral interactions between
722 adsorbed species in multicomponent systems (Teodoro et al., 2017). Positive values of α
723 indicated that oxyanions of Cr(VI) or Cu(II) ions did not tend to adsorb near other
724 adsorbed species on the C1 surface, which could be explained by repulsive potentials
725 around species adsorbed on the surface. The value of α was higher for Cr(VI) adsorption
726 than for Cu(II) adsorption, suggesting that oxyanions of Cr(VI) tended not to adsorb near
727 Cu(II) ions already adsorbed on C1 surface sites. In contrast, positive values of β
728 indicated that oxyanions of Cr(VI) or Cu(II) ions tended to desorb from the C1 surface
729 when it became progressively saturated. The higher value of β for Cr(VI) adsorption,
730 compared to Cu(II) adsorption, showed that oxyanions of Cr(VI) tended to desorb from
731 the C1 surface faster than Cu(II) ions. According to Cuypers et al. (1987), the greater the
732 sum of the interaction constants ($\gamma = \alpha + \beta$), the greater the effect of a solute i on the
733 adsorption of a solute j . At pH 4.5, the oxyanions of Cr(VI) had a greater influence on
734 Cu(II) adsorption, compared to the influence of Cu(II) adsorption on the adsorption of
735 oxyanions of Cr(VI). This was in agreement with the results obtained for the simultaneous
736 adsorption (at pH 4.5) of oxyanions of Cr(VI) ($q_{\text{multi}}/q_{\text{mono}} = 0.8$) and Cu(II)
737 ($q_{\text{multi}}/q_{\text{mono}} = 2.6$).

738 In the bicomponent adsorption, oxyanions of Cr(VI) presented a 3-fold higher effective
739 diffusion coefficient (D_i), compared to Cu(II) ions. The thickness of the unstirred water
740 layer (δ) surrounding the **C1** particles seemed to have a significant effect on the
741 adsorption of Cu(II) ions and oxyanions of Cr(VI) on **C1**. The diameter of a water
742 molecule is 0.278 nm (Zou et al., 2007), so the estimated thickness of the unstirred water
743 layer was ~ 62 water molecules.

744 **Table 5**

745 **4.3.3. Adsorption of Cu(II) and oxyanions of Cr(VI) on C1, as a function of initial**
746 **metal ion concentration**

747 Multicomponent isotherms are useful for describing the adsorption behavior of a mixture
748 of solutes on an adsorbent. These isotherms can also assist in elucidating the influence of
749 a solute i on the adsorption capacity of a solute j , as well as the selectivity of an adsorbent
750 for a specific solute in a mixture of N solutes.

751 The ideal adsorbed solution theory model (IAST) was proposed by Myers and Prausnitz
752 (1965) for describing the adsorption of a mixture of gases. Later, Radke and Prausnitz
753 (1972) extended this model to the liquid phase. However, IAST is not suitable for
754 describing the adsorption of solutes that present antagonistic or synergistic interactions
755 (non-ideal behavior). The real adsorbed solution theory (RAST) was proposed by Costa
756 et al. (1981). This model is an extension of the IAST model for describing the adsorption
757 of solutes that present non-ideal behavior.

758 The RAST model was also successfully employed to model experimental equilibrium
759 data for adsorption of the binary systems Cu(II)/Co(II), Cu(II)/Ni(II), and Co(II)/Ni(II)
760 on a carboxylated cellulose derivative (Teodoro et al., 2017) as well as the bicomponent

761 adsorption of auramine-O and safranin-T on trimellitated sugarcane bagasse (Fideles et
762 al., 2019).

763 Figure 5c shows the bicomponent isotherm for simultaneous adsorption of Cu(II) and
764 oxyanions of Cr(VI) on **C1**. The values of Q_{\max} for adsorption of Cu(II) and oxyanions of
765 Cr(VI) on **C1** were 1.13 ± 0.01 and 0.98 ± 0.01 mmol g⁻¹, respectively. The sum of the
766 Q_{\max} values was 2.11 ± 0.03 mmol g⁻¹. The sums of the q_e values (at pH 4.5) for mono-
767 and bicomponent adsorption of oxyanions of Cr(VI) and Cu(II), as a function of solution
768 pH, were 1.9 ± 0.1 and 1.96 ± 0.03 mmol g⁻¹, respectively. This indicated that there was
769 a slight increase in the total adsorption capacity for bicomponent adsorption, compared
770 to monocomponent adsorption.

771 The bicomponent isotherm profiles showed that the q_e values for adsorption of Cu(II) and
772 oxyanions of Cr(VI) on **C1** increased progressively with increasing equilibrium Cr(VI)
773 and Cu(II) concentrations, until reaching a plateau.

774 Figure 6a shows plots of $q_{e,\text{exp}}$ against $q_{e,\text{est}}$ for simultaneous adsorption of Cu(II) and
775 oxyanions of Cr(VI) on **C1**. The results indicated that the RAST-Sips model provided
776 better prediction of the adsorption of oxyanions of Cr(VI) ($R^2 = 0.987$, $\chi^2 = 0.296$,
777 $RSS = 0.057$), compared to the adsorption of Cu(II) ions ($R^2 = 0.924$, $\chi^2 = 1.139$,
778 $RSS = 0.292$). The RAST model assumes deviations from ideal behavior for the
779 adsorption of a solute present in a mixture of N solutes, compared to single component
780 adsorption. Therefore, the activity coefficient (γ) was introduced in the RAST model.

781 Figure 6b presents a graph of the experimental values of γ , as a function of reduced
782 spreading pressure (Ψ), for the simultaneous adsorption of oxyanions of Cr(VI) and Cu(II)
783 on **C1**. The values of γ for Cr(VI) and Cu(II) were higher than unity, indicating that the

784 adsorptions of oxyanions of Cr(VI) and Cu(II) on **C1** deviated from ideal behavior (Erto
785 et al., 2012; Teodoro et al., 2017).

786 Figure 6c presents a graph of the experimental values of γ_{Cr} , as a function of the
787 experimental values of γ_{Cu} , for the simultaneous adsorption of oxyanions of Cr(VI) and
788 Cu(II) on **C1**. Linear regression of the data resulted in a high R^2 value (> 0.98) and low
789 values of χ^2_{red} (5.76×10^{-5}) and RSS (8.06×10^{-4}), indicating that the Wilson model
790 equations (Wilson, 1964) could be used for estimating the adjustable parameters (c , A_{12} ,
791 and A_{21}) (Teodoro et al., 2017).

792 The values of the adjustable parameters of the Wilson model for simultaneous adsorption
793 of Cu(II) and oxyanions of Cr(VI) on **C1** ($i = 1 = \text{Cu(II)}$ and $j = 2 = (\text{Cr(VI)})$) were
794 $c = 0.8516$, $A_{12} = 1.2432$, $A_{21} = 1.1404$, $R_i^2 = 0.9372$, $R_j^2 = 0.9193$, and $RSS = 0.0127$.

795 The interaction parameters A_{12} and A_{21} of the Wilson model were used to evaluate the
796 effect of interaction between oxyanions of Cr(VI) and Cu(II) ions. The value of A_{12} was
797 greater than the value of A_{21} , indicating that Cu(II) ions had a greater influence on the
798 adsorption of oxyanions of Cr(VI) on **C1**, compared to the influence of oxyanions of
799 Cr(VI) on the adsorption of Cu(II) ions. This was in agreement with the results obtained
800 for the simultaneous adsorption of Cu(II) ions and oxyanions of Cr(VI), as a function of
801 solution pH.

802 **4.3.4. Energy dispersive X-ray spectroscopy (EDX)**

803 Figure 7 presents SEM-EDX images of the **C1** surface loaded with Cu(II), oxyanions of
804 Cr(VI), or both. Figures 7a and 7b show that the distributions of adsorbed Cr(VI) and
805 Cu(II) ions along the **C1** surface were not homogeneous. This was confirmed by EDX
806 microanalysis along lines with length of 1500 μm , drawn on the **C1** samples loaded with

807 Cr(VI) or Cu(II) ions (Supplementary Figure 4). The concentrations of Cu(II) ions or
808 oxyanions of Cr(VI) on the C1 surface were not constant along the line. Figure 7c shows
809 an SEM-EDX image of the C1 surface loaded with both Cr(VI) and Cu(II) ions present
810 in an equimolar mixture, revealing non-uniform distributions of Cr(VI) and Cu(II) ions
811 along the C1 surface. In addition, there appeared to be a number of vacant adsorption
812 sites on the C1 surface loaded with both Cr(VI) and Cu(II) ions, when compared to SEM-
813 EDX images of C1 loaded with either Cr(VI) (Figure 7a) or Cu(II) (Figure 7b) ions. Since
814 the total adsorption capacity of C1 for Cr(VI) and Cu(II) ions did not decrease (as pointed
815 out in Section 4.3.3), this was suggestive of cooperative adsorption between oxyanions
816 of Cr(VI) and Cu(II) on C1. This was in agreement with the hypothesis discussed in
817 Section 4.2.2, concerning the formation of a diffuse ion swarm.

818 **Figure 7**

819 **4.4. Desorption and reuse of spent adsorbent**

820 In Table 3 are presented the E_{des} values for the desorption of oxyanions of Cr(VI) and
821 Cu(II) from C1 using aqueous solutions of Na_2CO_3 (1.0 mol L^{-1}) and triethylenetetramine
822 (0.01 mol L^{-1}), respectively. The value of E_{des} for Cu(II) (~96%) was higher than for
823 Cr(VI) (~49%). The Cu(II) ions were almost completely desorbed from C1, because the
824 complex formed between Cu(II) and triethylenetetramine (trien) is highly stable.
825 Transition metals such as Cu(II) bind to the amine functions, forming polydentate
826 complexes of high stability (Navarro et al., 2001). The formation constant (K_1) of the
827 trien-Cu(II) complex has a high value, with $\log K_1$ of 20.4 at 25 °C (Dean and Lange,
828 1999).

829 The oxyanions of Cr(VI) were only partially desorbed from **C1**, presenting behavior
830 different to that observed for Cu(II) desorption. The desorption of oxyanions of Cr(VI)
831 was expected to occur by ion exchange, since the ions were adsorbed by electrostatic
832 attraction (outer-sphere complexes). The size of HCrO_4^- is 2.42 Å (Sharma and Forster,
833 1994), while the size of CO_3^{2-} is 1.85 Å (Chen et al., 2012). Although the charge/radius
834 (Z/r) ratio of HCrO_4^- (1/2.42) is higher than that of CO_3^{2-} (2/1.89), monovalent anions are
835 easily exchanged by multivalent anions. Therefore, the use of a desorbent such as
836 carbonate solution should enable the ion exchange of HCrO_4^- by CO_3^{2-} . On the other hand,
837 the partial desorption of oxyanions of Cr(VI) from different adsorbents has been reported
838 to be due to the phenomenon of aging (Kuo and Bembenek, 2008; Moreira et al., 2018).
839 According to Kuo and Bembenek (2008), oxyanions of Cr(VI) freshly loaded onto
840 adsorbents can be easily desorbed.

841 In Table 3 are presented the values of $E_{\text{re-ads}}$ for re-adsorption of oxyanions of Cr(VI) and
842 Cu(II) on the spent **C1** adsorbent. The value of $E_{\text{re-ads}}$ for Cr(VI) re-adsorption was ~36%.
843 This was expected, due to the low E_{des} value for Cr(VI) desorption from **C1**. After
844 desorption, a significant amount of oxyanions of Cr(VI) remained on the **C1** surface,
845 decreasing the number of free adsorption sites available for re-adsorption of Cr(VI)
846 species. Although the $E_{\text{re-ads}}$ value for Cr(VI) was considered low, this did not prevent the
847 reuse of **C1**, since the material was still able to adsorb oxyanions of Cr(VI). On the other
848 hand, the $E_{\text{re-ads}}$ value for Cu(II) was ~100%, showing that the spent **C1** adsorbent was
849 able to adsorb the same amount of Cu(II) ions as in the first adsorption cycle. This
850 demonstrated the excellent reuse potential of **C1** for the adsorption of cations.

851 **5. Conclusions**

852 The imine and pyridine groups introduced on **C1** were able to adsorb oxyanions of Cr(VI)
853 by the formation of outer-sphere complexes ($\Delta_{\text{ads}}H^{\circ} = -35.2 \pm 0.2$, $T\Delta_{\text{ads}}S^{\circ} = -14 \pm 3$),
854 while Cu(II) ions were adsorbed by the formation of inner-sphere complexes ($\Delta_{\text{ads}}H^{\circ} = -$
855 33.0 ± 0.8 , $T\Delta_{\text{ads}}S^{\circ} = -7 \pm 3$), as shown by the thermodynamic parameters of adsorption.
856 **C1** was able to simultaneously adsorb oxyanions of Cr(VI) and Cu(II) ions in the pH
857 range 3.6-5.5, showing the versatility of this material for water treatment. The maximum
858 adsorption capacities (at pH 4.5) of **C1** for oxyanions of Cr(VI) and Cu(II) ions were
859 0.98 ± 0.01 and 1.13 ± 0.01 mmol g⁻¹, respectively. Although **C1** was able to adsorb
860 Cu(II) and Cr(VI) simultaneously (at pH 3.6-4.5), better adsorption performance was
861 observed for single solute adsorption, with Q_{max} values of 3.8 ± 0.1 mmol g⁻¹ (at pH 3.6)
862 and 1.84 ± 0.03 mmol g⁻¹ (at pH 5.5) for Cr(VI) and Cu(II), respectively. The reuse of **C1**
863 was investigated, with Cu(II) ions being almost completely desorbed (~96%) and fully
864 re-adsorbed (~100%). For Cr(VI) ions, the desorption was incomplete (~49%), resulting
865 in low re-adsorption (~36%). **C1** was demonstrated to be an excellent adsorbent for
866 cations of Cu(II), while its use for adsorption of oxyanions of Cr(VI) was limited by its
867 partial reuse capacity.

868 **Acknowledgments**

869 The authors are grateful for research support provided by Universidade Federal de Ouro
870 Preto (UFOP), Fundação de Amparo à Pesquisa do Estado de Minas Gerais (FAPEMIG,
871 grant number CEX-APQ-01764-14), Conselho Nacional de Desenvolvimento Científico
872 e Tecnológico (CNPq PVE grant number 400739/2014-3, CNPq grant number
873 422507/2018-0, ANR (ANR-11-BS07-030-01)), LabEx CHARMMMAT (ANR-11-
874 LABEX-0039), and the University of Versailles St Quentin. The authors are also grateful
875 to FAPEMIG for a Master's scholarship awarded to F. J. Gonçalves.

876 **References**

- 877 Abou El-Reash, Y.G., 2016. Magnetic chitosan modified with cysteine-glutaraldehyde as
878 adsorbent for removal of heavy metals from water. *J. Environ. Chem. Eng.* 4,
879 3835-3847. <https://doi.org/10.1016/j.jece.2016.08.014>.
- 880 Adamczuk, A., Kołodyńska, D., 2015. Equilibrium, thermodynamic and kinetic studies
881 on removal of chromium, copper, zinc and arsenic from aqueous solutions onto
882 fly ash coated by chitosan. *Chem. Eng. J.* 274, 200-212.
883 <https://doi.org/10.1016/j.cej.2015.03.088>.
- 884 Ahmad, M., Manzoor, K., Ikram, S., 2017. Versatile nature of hetero-chitosan based
885 derivatives as biodegradable adsorbent for heavy metal ions; a review. *Int. J. Biol.*
886 *Macromol.* 105, 190-203. <https://doi.org/10.1016/j.ijbiomac.2017.07.008>.
- 887 Almeida, F.T.R.d., Ferreira, B.C.S., Moreira, A.L.d.S.L., Freitas, R.P.d., Gil, L.F.,
888 Gurgel, L.V.A., 2016. Application of a new bifunctionalized chitosan derivative
889 with zwitterionic characteristics for the adsorption of Cu^{2+} , Co^{2+} , Ni^{2+} , and
890 oxyanions of Cr^{6+} from aqueous solutions: Kinetic and equilibrium aspects. *J.*
891 *Colloid Interf. Sci.* 466, 297-309. <http://dx.doi.org/10.1016/j.jcis.2015.12.037>.
- 892 Anush, S.M., Vishalakshi, B., 2019. Modified chitosan gel incorporated with magnetic
893 nanoparticle for removal of Cu(II) and Cr(VI) from aqueous solution. *Int. J. Biol.*
894 *Macromol.* 133, 1051-1062. <https://doi.org/10.1016/j.ijbiomac.2019.04.179>.
- 895 ATSDR, 2011. Toxic Substances Portal - Arsenic. CCA -Treated Wood, Division of
896 Toxicology and Human Health Sciences, Atlanta, GA, USA.
- 897 Ayres, R.U., Ayres, L.W., Råde, I., 2003. *The Life Cycle of Copper, Its Co-Products and*
898 *Byproducts*, 1st ed. Springer Netherlands.

899 Barrett, E.P., Joyner, L.G., Halenda, P.P., 1951. The Determination of Pore Volume and
900 Area Distributions in Porous Substances. I. Computations from Nitrogen
901 Isotherms. J. Am. Chem. Soc. 73, 373-380. <https://doi.org/10.1021/ja01145a126>.

902 Boyd, G.E., Adamson, A.W., Myers, L.S., 1947. The exchange adsorption of ions from
903 aqueous solutions by organic zeolites. II. Kinetics. J. Am. Chem. Soc. 69, 2836-
904 2848. <https://doi.org/10.1021/ja01203a066>.

905 Brown, G.E., Parks, G.A., O'Day, P.A., 1995. Sorption at mineral-water interfaces:
906 Macroscopic and microscopic perspectives, in: Vaughan, D.J., Patrick, R.A.D.,
907 editors(Eds.), Mineral surfaces. Chapman & Hall, London, pp. 129-183.

908 Brunauer, S., Emmett, P.H., Teller, E., 1938. Adsorption of gases in multimolecular
909 layers. J. Am. Chem. Soc. 60, 309-319. <https://doi.org/10.1021/ja01269a023>.

910 Chen, J., Song, D., Yang, P., 2016. Study on adsorption of Cu(II)–Cr(VI) binary system
911 by carbonized *Eupatorium adenophorum*. Sep. Sci. Technol. 51, 749-758.
912 <https://doi.org/10.1080/01496395.2015.1131720>.

913 Chen, J., Song, Y., Shan, D., Han, E.-H., 2012. Study of the corrosion mechanism of the
914 in situ grown Mg–Al–CO₃²⁻ hydroxalite film on AZ31 alloy. Corros. Sci. 65,
915 268-277. <https://doi.org/10.1016/j.corsci.2012.08.026>.

916 Choudhary, S., Goyal, V., Singh, S., 2015. Removal of copper(II) and chromium(VI)
917 from aqueous solution using sorghum roots (*S. bicolor*): a kinetic and
918 thermodynamic study. Clean Technol. Envir. 17, 1039-1051.
919 <https://doi.org/10.1007/s10098-014-0860-2>.

920 Corsel, J.W., Willems, G.M., Kop, J.M.M., Cuypers, P.A., Hermens, W.T., 1986. The
921 role of intrinsic binding rate and transport rate in the adsorption of prothrombin,
922 albumin, and fibrinogen to phospholipid bilayers. J. Colloid Interf. Sci. 111, 544-
923 554. [http://dx.doi.org/10.1016/0021-9797\(86\)90058-5](http://dx.doi.org/10.1016/0021-9797(86)90058-5).

924 Costa, E., Sotelo, J.L., Calleja, G., Marrón, C., 1981. Adsorption of binary and ternary
925 hydrocarbon gas mixtures on activated carbon: Experimental determination and
926 theoretical prediction of the ternary equilibrium data. *AIChE Journal*. 27, 5-12.
927 <https://doi.org/10.1002/aic.690270103>.

928 Cuypers, P.A., Willems, G.M., Hemker, H.C., Hermens, W.T., 1987. Adsorption kinetics
929 of protein mixtures. A tentative explanation of the Vroman effect. *Ann. N.Y.*
930 *Acad. Sci.* 516, 244-252. <https://doi.org/10.1111/j.1749-6632.1987.tb33045.x>.

931 De Gisi, S., Lofrano, G., Grassi, M., Notarnicola, M., 2016. Characteristics and
932 adsorption capacities of low-cost sorbents for wastewater treatment: A review.
933 *Sustainable Materials and Technologies*. 9, 10-40.
934 <https://doi.org/10.1016/j.susmat.2016.06.002>.

935 Dean, J.A., Lange, N.A., 1999. *Lange's Handbook of chemistry*, 15th ed. McGraw-Hill,
936 New York, USA.

937 Debye, P., Hückel, E., 1923. Zur Theorie der Elektrolyte. I. Gefrierpunktniedrigung
938 und verwandte Erscheinungen. *Physikalische Zeitschrift*. 24, 185–206.

939 Divya, K., Jisha, M.S., 2018. Chitosan nanoparticles preparation and applications.
940 *Environ Chem Lett*. 16, 101-112. <https://doi.org/10.1007/s10311-017-0670-y>.

941 Dong, A., Xie, J., Wang, W., Yu, L., Liu, Q., Yin, Y., 2010. A novel method for amino
942 starch preparation and its adsorption for Cu(II) and Cr(VI). *J. Hazard. Mater.* 181,
943 448-454. <https://doi.org/10.1016/j.jhazmat.2010.05.031>.

944 Elias, M.M.C., Ferreira, G.M.D., de Almeida, F.T.R., Rosa, N.C.M., Silva, I.A.,
945 Filgueiras, J.G., de Azevedo, E.R., da Silva, L.H.M., Melo, T.M.S., Gil, L.F.,
946 Gurgel, L.V.A., 2019. Synthesis and application of sugarcane bagasse cellulose
947 mixed esters. Part I: Removal of Co²⁺ and Ni²⁺ from single spiked aqueous

948 solutions in batch mode using sugarcane bagasse cellulose succinate phthalate. J.
949 Colloid Interf. Sci. 533, 678-691. <https://doi.org/10.1016/j.jcis.2018.08.109>.

950 Erto, A., Lancia, A., Musmarra, D., 2012. A Real Adsorbed Solution Theory model for
951 competitive multicomponent liquid adsorption onto granular activated carbon.
952 Micropor. Mesopor. Mat. 154, 45-50.
953 <http://dx.doi.org/10.1016/j.micromeso.2011.10.041>.

954 Fida, H., Guo, S., Zhang, G., 2015. Preparation and characterization of bifunctional Ti-
955 Fe kaolinite composite for Cr(VI) removal. J. Colloid Interf. Sci. 442, 30-38.
956 <https://doi.org/10.1016/j.jcis.2014.11.023>.

957 Fideles, R.A., Teodoro, F.S., Xavier, A.L.P., Adarme, O.F.H., Gil, L.F., Gurgel, L.V.A.,
958 2019. Trimellitated sugarcane bagasse: A versatile adsorbent for removal of
959 cationic dyes from aqueous solution. Part II: Batch and continuous adsorption in
960 a bicomponent system. J. Colloid Interf. Sci. 552, 752-763.
961 <https://doi.org/10.1016/j.jcis.2019.05.089>.

962 Goncalves, F.J., Kamal, F., Gaucher, A., Gil, R., Bourdreux, F., Martineau-Corcus, C.,
963 Gurgel, L.V.A., Gil, L.F., Prim, D., 2018. Synthesis, characterisation and
964 application of pyridine-modified chitosan derivatives for the first non-racemic
965 Cu-catalysed Henry reaction. Carbohydr. Polym. 181, 1206-1212.
966 <https://doi.org/10.1016/j.carbpol.2017.12.012>.

967 Harris, D.C., 2010. Quantitative Chemical Analysis, 8th ed. W. H. Freeman, New York,
968 USA.

969 Haynes, W.M., Lide, D.R., Bruno, T.J., 2014. CRC Handbook of Chemistry and Physics,
970 95th ed. Taylor & Francis, Boca Raton, FL, USA.

971 Ho, Y.S., McKay, G., 1999. Pseudo-second order model for sorption processes. Process
972 Biochem. 34, 451-465. [http://dx.doi.org/10.1016/S0032-9592\(98\)00112-5](http://dx.doi.org/10.1016/S0032-9592(98)00112-5).

973 Kumar, R., Barakat, M.A., Taleb, M.A., Seliem, M.K., 2020. A recyclable
974 multifunctional graphene oxide/SiO₂@polyaniline microspheres composite for
975 Cu(II) and Cr(VI) decontamination from wastewater. *J. Clean Prod.* 268, 122290.
976 <https://doi.org/10.1016/j.jclepro.2020.122290>.

977 Kuo, S., Bembenek, R., 2008. Sorption and desorption of chromate by wood shavings
978 impregnated with iron or aluminum oxide. *Bioresour. Technol.* 99, 5617-5625.
979 <https://doi.org/10.1016/j.biortech.2007.10.062>.

980 Kurita, K., 2001. Controlled functionalization of the polysaccharide chitin. *Prog Polym*
981 *Sci.* 26, 1921-1971. [http://dx.doi.org/10.1016/S0079-6700\(01\)00007-7](http://dx.doi.org/10.1016/S0079-6700(01)00007-7).

982 Kyzas, G.Z., Bikiaris, D.N., Mitropoulos, A.C., 2017. Chitosan adsorbents for dye
983 removal: a review. *Polym. Int.* 66, 1800-1811. <https://doi.org/10.1002/pi.5467>.

984 Lagergren, S.Y., 1898. Zur theorie der sogenannten adsorption gelöster stoffe, *kungliga*
985 *svenska vetenskapsakademiens. Handlingar.* 24, 1-39.

986 Langmuir, I., 1918. The adsorption of gases on plane surfaces of glass, mica and platinum.
987 *J. Am. Chem. Soc.* 40, 1361-1403. <https://doi.org/10.1021/ja02242a004>.

988 Li, R., Liang, W., Huang, H., Jiang, S., Guo, D., Li, M., Zhang, Z., Ali, A., Wang, J.J.,
989 2018. Removal of cadmium(II) cations from an aqueous solution with
990 aminothiourea chitosan strengthened magnetic biochar. *J. Appl. Polym. Sci.* 135,
991 46239. <https://doi.org/10.1002/app.46239>.

992 Li, Y., Xu, C., Qiu, T., Xu, X., 2015. Crosslinked electro-spun chitosan nanofiber mats
993 with Cd(II) as template ions for adsorption applications. *J. Nanosci. Nanotechno.*
994 15, 4245-54. <https://doi.org/10.1166/jnn.2015.10197>.

995 Liu, Y., 2009. Is the free energy change of adsorption correctly calculated? *J. Chem. Eng.*
996 *Data.* 54, 1981-1985. <https://doi.org/10.1021/Je800661q>.

997 Lv, L., He, J., Wei, M., Evans, D.G., Duan, X., 2006. Factors influencing the removal of
998 fluoride from aqueous solution by calcined Mg–Al–CO₃ layered double
999 hydroxides. *J. Hazard. Mater.* 133, 119-128.
1000 <https://doi.org/10.1016/j.jhazmat.2005.10.012>.

1001 Marcus, Y., 1987a. Solvent release upon ion association from entropy data. *J Solution*
1002 *Chem.* 16, 735-744. <https://doi.org/10.1007/BF00652576>.

1003 Marcus, Y., 1987b. The thermodynamics of solvation of ions. Part 2. The enthalpy of
1004 hydration at 298.15 K. *J. Chem. Soc., Faraday Trans. 1 F.* 83, 339-349.
1005 <https://doi.org/10.1039/F19878300339>.

1006 Moreira, A.L.d.S.L., Pereira, A.d.S., Speziali, M.G., Novack, K.M., Gurgel, L.V.A., Gil,
1007 L.F., 2018. Bifunctionalized chitosan: A versatile adsorbent for removal of Cu(II)
1008 and Cr(VI) from aqueous solution. *Carbohydr. Polym.* 201, 218-227.
1009 <https://doi.org/10.1016/j.carbpol.2018.08.055>.

1010 Morrison, R.D., Murphy, B.L., 2010. *Environmental Forensics: Contaminant Specific*
1011 *Guide*, 1st ed. Academic Press, USA.

1012 Mosa, K.A., Saadoun, I., Kumar, K., Helmy, M., Dhankher, O.P., 2016. Potential
1013 biotechnological strategies for the cleanup of heavy metals and metalloids. *Front*
1014 *Plant Sci.* 7, 303-303. <https://doi.org/10.3389/fpls.2016.00303>.

1015 Motzer, W.E., 2004. Chemistry, Geochemistry, and Geology of Chromium and
1016 Chromium Compounds, in: Guertin, J., Jacobs, J.A., Avakian, C.P., editors(Eds.),
1017 Chromium(VI) Handbook. 1st edition. CRC Press, Boca Raton, FL, USA, pp. 23-
1018 92.

1019 Mulligan, C., Bronstein, J.M., 2020. Wilson Disease: An Overview and Approach to
1020 Management. *Neurol. Clin.* 38, 417-432.
1021 <https://doi.org/10.1016/j.ncl.2020.01.005>.

1022 Myers, A.L., 1983. Activity coefficients of mixtures adsorbed on heterogeneous surfaces.
1023 AICHE Journal. 29, 691-693. <https://doi.org/10.1002/aic.690290428>.

1024 Myers, A.L., Prausnitz, J.M., 1965. Thermodynamics of mixed-gas adsorption. AICHE
1025 Journal. 11, 121-127. <https://doi.org/10.1002/aic.690110125>.

1026 Navarro, R.R., Tatsumi, K., Sumi, K., Matsumura, M., 2001. Role of anions on heavy
1027 metal sorption of a cellulose modified with poly(glycidyl methacrylate) and
1028 polyethyleneimine. Water Res. 35, 2724-2730. [https://doi.org/10.1016/S0043-
1029 1354\(00\)00546-7](https://doi.org/10.1016/S0043-1354(00)00546-7).

1030 Neeli, S.T., Ramsurn, H., Ng, C.Y., Wang, Y., Lu, J., 2020. Removal of Cr (VI), As (V),
1031 Cu (II), and Pb (II) using cellulose biochar supported iron nanoparticles: A kinetic
1032 and mechanistic study. J. Environ. Chem. Eng. 8, 103886.
1033 <https://doi.org/10.1016/j.jece.2020.103886>.

1034 Nightingale, E.R., 1959. Phenomenological theory of ion solvation. Effective radii of
1035 hydrated ions. J. Phys. Chem. 63, 1381-1387.
1036 <https://doi.org/10.1021/j150579a011>.

1037 Noh, J.S., Schwarz, J.A., 1990. Effect of HNO₃ treatment on the surface-acidity of
1038 activated carbons. Carbon. 28, 675-682. [https://doi.org/10.1016/0008-
1039 6223\(90\)90069-B](https://doi.org/10.1016/0008-6223(90)90069-B).

1040 NPIC, 2014. Chromated Copper Arsenate (CCA) Wood Preservatives, Oregon State
1041 University, Corvallis, OR, USA.

1042 O'Connell, D.W., Birkinshaw, C., O'Dwyer, T.F., 2008. Heavy metal adsorbents
1043 prepared from the modification of cellulose: A review. Bioresour. Technol. 99,
1044 6709-6724. <http://dx.doi.org/10.1016/j.biortech.2008.01.036>.

1045 Plazinski, W., Dziuba, J., Rudzinski, W., 2013. Modeling of sorption kinetics: the pseudo-
1046 second order equation and the sorbate intraparticle diffusivity. *Adsorption*. 19,
1047 1055-1064. <https://doi.org/10.1007/s10450-013-9529-0>.

1048 Plazinski, W., Rudzinski, W., Plazinska, A., 2009. Theoretical models of sorption kinetics
1049 including a surface reaction mechanism: A review. *Adv. Colloid Interface Sci.*
1050 152, 2-13. <http://dx.doi.org/10.1016/j.cis.2009.07.009>.

1051 Purkayastha, D., Mishra, U., Biswas, S., 2014. A comprehensive review on Cd(II)
1052 removal from aqueous solution. *J Water Process Eng.* 2, 105-128.
1053 <https://doi.org/10.1016/j.jwpe.2014.05.009>.

1054 Radke, C.J., Prausnitz, J.M., 1972. Thermodynamics of multi-solute adsorption from
1055 dilute liquid solutions. *AIChE Journal.* 18, 761-768.
1056 <https://doi.org/10.1002/aic.690180417>.

1057 Rahimi, K., Mirzaei, R., Akbari, A., Mirghaffari, N., 2018. Preparation of nanoparticle-
1058 modified polymeric adsorbent using wastage fuzzes of mechanized carpet and its
1059 application in dye removal from aqueous solution. *J. Clean Prod.* 178, 373-383.
1060 <https://doi.org/10.1016/j.jclepro.2017.12.213>.

1061 Rahman, N., Hossen, M.S., Miah, A.R., Marjub, M.M., Dafader, N.C., Shahnaz, S.,
1062 Alam, M.F., 2019. Removal of Cu(II), Pb(II) and Cr(VI) ions from aqueous
1063 solution using amidoximated non-woven polyethylene-g-acrylonitrile fabric. *J.*
1064 *Environ. Health Sci.* 17, 183-194. <https://doi.org/10.1007/s40201-019-00339-0>.

1065 Ramos, S.N.d.C., Xavier, A.L.P., Teodoro, F.S., Elias, M.M.C., Gonçalves, F.J., Gil,
1066 L.F., de Freitas, R.P., Gurgel, L.V.A., 2015. Modeling mono- and multi-
1067 component adsorption of cobalt(II), copper(II), and nickel(II) metal ions from
1068 aqueous solution onto a new carboxylated sugarcane bagasse. Part I: Batch

1069 adsorption study. Ind. Crop. Prod. 74, 357-371.
1070 <http://dx.doi.org/10.1016/j.indcrop.2015.05.022>.

1071 Redlich, O., Peterson, D.L., 1959. A useful adsorption isotherm. J. Phys. Chem. 63, 1024-
1072 1024. <https://doi.org/10.1021/j150576a611>.

1073 Sarkar, M., Rahman, A., Islam, J., Ahmed, K., Uddin, M., Bhoumik, N., 2015. Study of
1074 hydrochemistry and pollution status of the Buriganga river, Bangladesh.
1075 Bangladesh Journal of Scientific and Industrial Research. 50, 123-134.
1076 <https://doi.org/10.3329/bjsir.v50i2.24353>.

1077 Sarkar, M., Rahman, A.K.M.L., Bhoumik, N.C., 2017. Remediation of chromium and
1078 copper on water hyacinth (*E. crassipes*) shoot powder. Water Resour. Ind. 17, 1-
1079 6. <https://doi.org/10.1016/j.wri.2016.12.003>.

1080 Shanthi, T., Selvarajan, V.M., 2013. Removal of Cr(VI) and Cu(II) Ions from Aqueous
1081 Solution by Carbon Prepared from Henna Leaves. J. Chem. 2013, 304970.
1082 <https://doi.org/10.1155/2013/304970>.

1083 Sharma, D.C., Forster, C.F., 1994. The treatment of chromium wastewaters using the
1084 sorptive potential of leaf mould. Bioresour. Technol. 49, 31-40.
1085 [https://doi.org/10.1016/0960-8524\(94\)90170-8](https://doi.org/10.1016/0960-8524(94)90170-8).

1086 Shen, H., Pan, S., Zhang, Y., Huang, X., Gong, H., 2012. A new insight on the adsorption
1087 mechanism of amino-functionalized nano-Fe₃O₄ magnetic polymers in Cu(II),
1088 Cr(VI) co-existing water system. Chem. Eng. J. 183, 180-191.
1089 <https://doi.org/10.1016/j.cej.2011.12.055>.

1090 Silva-Yumi, J., Escudey, M., Gacitua, M., Pizarro, C., 2018. Kinetics, adsorption and
1091 desorption of Cd(II) and Cu(II) on natural allophane: Effect of iron oxide coating.
1092 Geoderma. 319, 70-79. <https://doi.org/10.1016/j.geoderma.2017.12.038>.

1093 Sips, R., 1948. On the structure of a catalyst surface. *J. Chem. Phys.* 16, 490-495.
1094 <http://dx.doi.org/10.1063/1.1746922>.

1095 Sposito, G., 2008. *The Chemistry of Soils*, ed. Oxford University Press, New York, USA.

1096 Sudha Bai, R., Abraham, T.E., 2003. Studies on chromium(VI) adsorption–desorption
1097 using immobilized fungal biomass. *Bioresour. Technol.* 87, 17-26.
1098 [https://doi.org/10.1016/S0960-8524\(02\)00222-5](https://doi.org/10.1016/S0960-8524(02)00222-5).

1099 Talu, O., Zwiebel, I., 1986. Multicomponent adsorption equilibria of nonideal mixtures.
1100 *AIChE Journal.* 32, 1263-1276. <https://doi.org/10.1002/aic.690320805>.

1101 Teodoro, F.S., Adarme, O.F.H., Gil, L.F., Gurgel, L.V.A., 2017. Synthesis and
1102 application of a new carboxylated cellulose derivative. Part II: Removal of Co^{2+} ,
1103 Cu^{2+} and Ni^{2+} from bicomponent spiked aqueous solution. *J. Colloid Interf. Sci.*
1104 487, 266-280. <http://dx.doi.org/10.1016/j.jcis.2016.10.043>.

1105 Teodoro, F.S., Elias, M.M.C., Ferreira, G.M.D., Adarme, O.F.H., Savedra, R.M.L.,
1106 Siqueira, M.F., da Silva, L.H.M., Gil, L.F., Gurgel, L.V.A., 2018. Synthesis and
1107 application of a new carboxylated cellulose derivative. Part III: Removal of
1108 auramine-O and safranin-T from mono- and bi-component spiked aqueous
1109 solutions. *J. Colloid Interf. Sci.* 512, 575-590.
1110 <https://doi.org/10.1016/j.jcis.2017.10.083>.

1111 Teodoro, F.S., Ramos, S.N.d.C., Elias, M.M.C., Mageste, A.B., Ferreira, G.M.D., da
1112 Silva, L.H.M., Gil, L.F., Gurgel, L.V.A., 2016. Synthesis and application of a new
1113 carboxylated cellulose derivative. Part I: Removal of Co^{2+} , Cu^{2+} and Ni^{2+} from
1114 monocomponent spiked aqueous solution. *J. Colloid Interf. Sci.* 483, 185-200.
1115 <http://dx.doi.org/10.1016/j.jcis.2016.08.004>.

1116 Uddin, M.K., 2017. A review on the adsorption of heavy metals by clay minerals, with
1117 special focus on the past decade. Chem. Eng. J. 308, 438-462.
1118 <https://doi.org/10.1016/j.ccej.2016.09.029>.

1119 Wan Ngah, W.S., Teong, L.C., Hanafiah, M.A.K.M., 2011. Adsorption of dyes and heavy
1120 metal ions by chitosan composites: A review. Carbohydr. Polym. 83, 1446-1456.
1121 <http://dx.doi.org/10.1016/j.carbpol.2010.11.004>.

1122 Wang, Y., Yu, L., Wang, R., Wang, Y., Zhang, X., 2020. A novel cellulose hydrogel
1123 coating with nanoscale Fe⁰ for Cr(VI) adsorption and reduction. Sci. Total
1124 Environ. 726, 138625. <https://doi.org/10.1016/j.scitotenv.2020.138625>.

1125 Weber, W.J., Morris, J.C., 1963. Kinetics of adsorption on carbon from solution. J. San.
1126 Eng. Div. 89, 31-60.

1127 WHO, 1996a. Chromium in Drinking-water. Background document for development of
1128 WHO Guidelines for Drinking-water Quality: Guidelines for drinking-water
1129 quality, 2nd ed. World Health Organization, Geneva, Switzerland.

1130 WHO, 1996b. Copper in Drinking-water. Background document for development of
1131 WHO Guidelines for Drinking-water Quality: Guidelines for drinking-water
1132 quality, 2nd ed. World Health Organization, Geneva, Switzerland.

1133 Wilbur, S., Abadin, H., Fay, M., Yu, D., Tencza, B., 2012. Toxicological profile for
1134 chromium, ed. US Department of Health and Human Services, Public Health
1135 Service, Agency for Toxic Substances and Disease Registry, Atlanta, USA.

1136 Wilson, G.M., 1964. Vapor-Liquid equilibrium. XI. A new expression for the excess free
1137 energy of mixing. J. Am. Chem. Soc. 86, 127-130.
1138 <https://doi.org/10.1021/ja01056a002>.

1139 Wu, F.-C., Tseng, R.-L., Juang, R.-S., 2010. A review and experimental verification of
1140 using chitosan and its derivatives as adsorbents for selected heavy metals. J.
1141 Environ. Manage. 91, 798-806. <http://dx.doi.org/10.1016/j.jenvman.2009.10.018>.

1142 Wu, R.X., Zheng, G.F., Li, W.W., Zhong, L.B., Zheng, Y.M., 2018. Electrospun chitosan
1143 nanofiber membrane for adsorption of Cu(II) from aqueous solution: Fabrication,
1144 characterization and performance. J. Nanosci. Nanotechno. 18, 5624-5635.
1145 <https://doi.org/10.1166/jnn.2018.15433>.

1146 Xin, S., Zeng, Z., Zhou, X., Luo, W., Shi, X., Wang, Q., Deng, H., Du, Y., 2017.
1147 Recyclable *Saccharomyces cerevisiae* loaded nanofibrous mats with sandwich
1148 structure constructing via bio-electrospraying for heavy metal removal. J. Hazard.
1149 Mater. 324, 365-372. <https://doi.org/10.1016/j.jhazmat.2016.10.070>.

1150 Xu, Q., Wang, Y., Jin, L., Wang, Y., Qin, M., 2017. Adsorption of Cu (II), Pb (II) and Cr
1151 (VI) from aqueous solutions using black wattle tannin-immobilized
1152 nanocellulose. J. Hazard. Mater. 339, 91-99.
1153 <https://doi.org/10.1016/j.jhazmat.2017.06.005>.

1154 Yan, R., Luo, D., Fu, C., Tian, W., Wu, P., Wang, Y., Zhang, H., Jiang, W., 2020.
1155 Simultaneous Removal of Cu(II) and Cr(VI) Ions from Wastewater by
1156 Photoreduction with TiO₂-ZrO₂. J Water Process Eng. 33, 101052.
1157 <https://doi.org/10.1016/j.jwpe.2019.101052>.

1158 Yu, Z., Song, W., Li, J., Li, Q., 2020. Improved simultaneous adsorption of Cu(II) and
1159 Cr(VI) of organic modified metakaolin-based geopolymer. Arabian J. Chem. 13,
1160 4811-4823. <https://doi.org/10.1016/j.arabjc.2020.01.001>.

1161 Zou, C., Fothergill, J.C., Rowe, S.W. A "water shell" model for the dielectric properties
1162 of hydrated silica-filled epoxy nano-composites. 2007 IEEE International
1163 Conference on Solid Dielectrics, 2007, pp. 389-392.

1165 **Figure 1.** Scheme illustrating (a) the synthesis of **C1** from chitosan and pyridine-2-
1166 carbaldehyde, and (b) the suggested mechanism for removal of Cu(II) and an oxyanion
1167 of Cr(VI) (HCrO_4^-) by the **C1** adsorbent.

1168 **Figure 2.** SEM images of chitosan (a and c) and **C1** (b and d) at 60 \times and 3,000 \times
1169 magnifications.

1170 **Figure 3.** Profiles of the adsorption capacity, as a function of (a) solution pH for
1171 adsorption of Cu(II) and Cr(VI), (b) contact time for the adsorption of Cu(II), (c) contact
1172 time for the adsorption of Cr(VI), (d) equilibrium solute concentration for adsorption of
1173 Cu(II), and (e) equilibrium solute concentration for adsorption of Cr(VI). Experimental
1174 conditions: (a) $[\text{Cu(II)}] = [\text{Cr(VI)}] = 0.77 \text{ mmol L}^{-1}$, 130 rpm, 25 $^\circ\text{C}$, 0.2 g L $^{-1}$ **C1**, and
1175 360 min contact time; (b) and (c) ($[\text{Cu(II)}] = [\text{Cr(VI)}] = 0.77 \text{ mmol L}^{-1}$, 130 rpm, 25 $^\circ\text{C}$,
1176 0.2 g L $^{-1}$ **C1**, pH 5.5 for Cu(II), and pH 3.6 for Cr(VI)); and (d) and (e): 130 rpm, 25 $^\circ\text{C}$,
1177 0.2 g L $^{-1}$ **C1**, pH 5.5 and 360 min for Cu(II), and pH 3.6 and 240 min for Cr(VI).

1178 **Figure 4.** Changes in enthalpy of adsorption, as a function of q_e , for adsorption on **C1** of
1179 Cu(II) at pH 5.5 and oxyanions of Cr(VI) at pH 3.6, at 25 $^\circ\text{C}$.

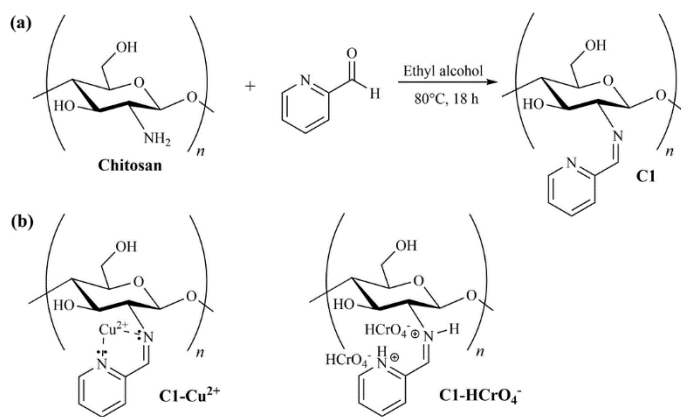
1180 **Figure 5.** Profiles of the simultaneous adsorption of Cu(II) and Cr(VI) on **C1**: (a)
1181 adsorption capacity as a function of solution pH, (b) adsorption capacity normalized by
1182 the specific surface area ($I(t)$), as a function of contact time, and (c) equilibrium
1183 adsorption capacity (q_e), as a function of equilibrium solute concentration. Experimental
1184 conditions: (a) 25 $^\circ\text{C}$, 130 rpm, $[\text{Cu(II)}] = [\text{Cr(VI)}] = 0.77 \text{ mmol L}^{-1}$, 0.2 g L $^{-1}$ **C1**, and
1185 180 min contact time; (b) $[\text{Cu(II)}] = [\text{Cr(VI)}] = 0.77 \text{ mmol L}^{-1}$, 130 rpm, 25 $^\circ\text{C}$,
1186 0.2 g L $^{-1}$ **C1**, pH 5.5 for Cu(II), and pH 3.6 for Cr(VI); and (c) 130 rpm, 25 $^\circ\text{C}$, 0.2 g L $^{-1}$
1187 **C1**, pH 4.5, and 180 min contact time.

1188 **Figure 6.** Plots for simultaneous adsorption of oxyanions of Cr(VI) and Cu(II) on **C1** of
1189 (a) experimental equilibrium adsorption capacity ($q_{e,\text{exp}}$) against estimated equilibrium
1190 adsorption capacity ($q_{e,\text{est}}$); (b) experimental activity coefficients of Cu(II) and Cr(VI), as
1191 a function of reduced spreading pressure, and (c) experimental activity coefficient of
1192 Cr(VI) plotted against experimental activity coefficient of Cu(II). Experimental
1193 conditions: (a) $[\text{Cu(II)}]_0 = [\text{Cr(VI)}]_0 = 0.05\text{-}4.0 \text{ mmol L}^{-1}$, 180 min, 25 $^\circ\text{C}$, pH 4.5,
1194 130 rpm, and 0.2 g L $^{-1}$ **C1**.

1195 **Figure 7.** SEM-EDX images with surface mapping for (a) oxyanions of Cr(VI), (b)
1196 Cu(II), and (c) oxyanions of Cr(VI) and Cu(II) adsorbed on **C1** ($[\text{Cu(II)}] = [\text{Cr(VI)}] =$
1197 0.77 mmol L^{-1} , 130 rpm, 25 $^\circ\text{C}$, 0.2 g L $^{-1}$ **C1**, 360 and 240 min contact times for
1198 individual adsorptions of Cu(II) and Cr(VI), respectively, and 180 min contact time for
1199 simultaneous adsorption of Cu(II) and Cr(VI)).

1200

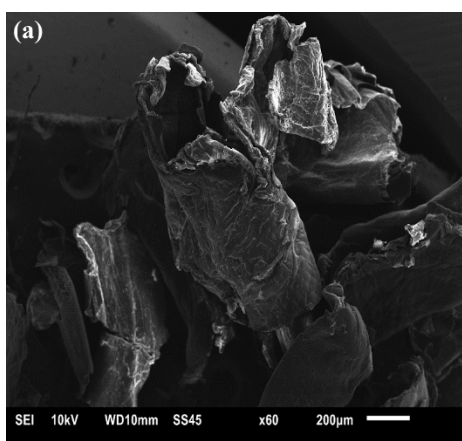
1201



1202

1203 Figure 1.

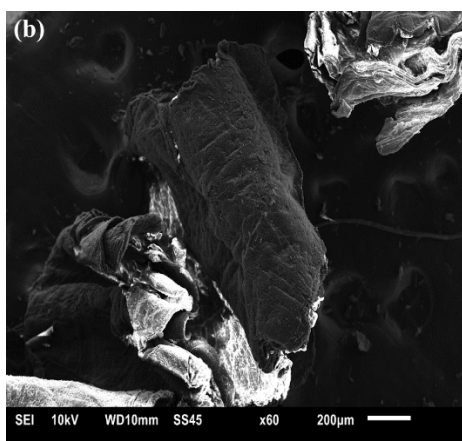
1204



1205

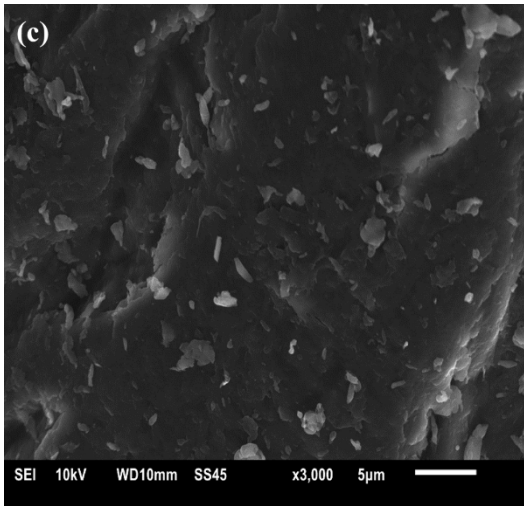
1206 Figure 2a

1207



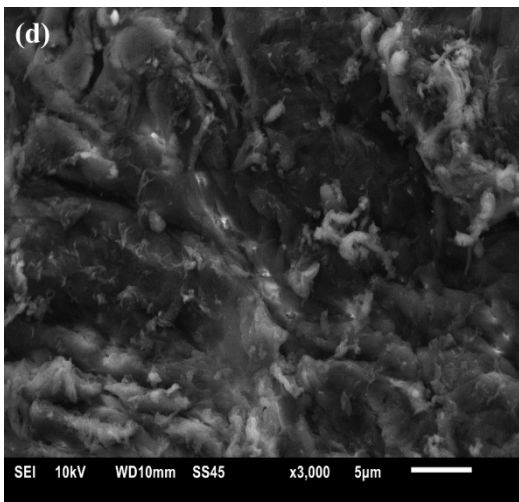
1208

1209 Figure 2b



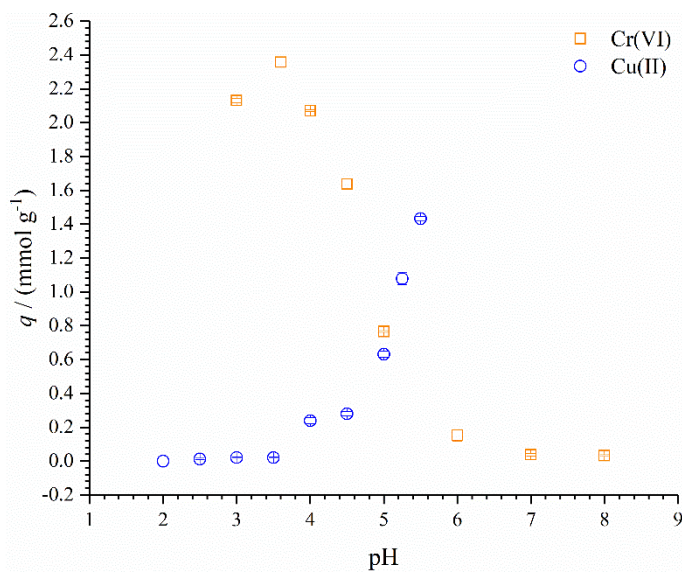
1210

1211 Figure 2c



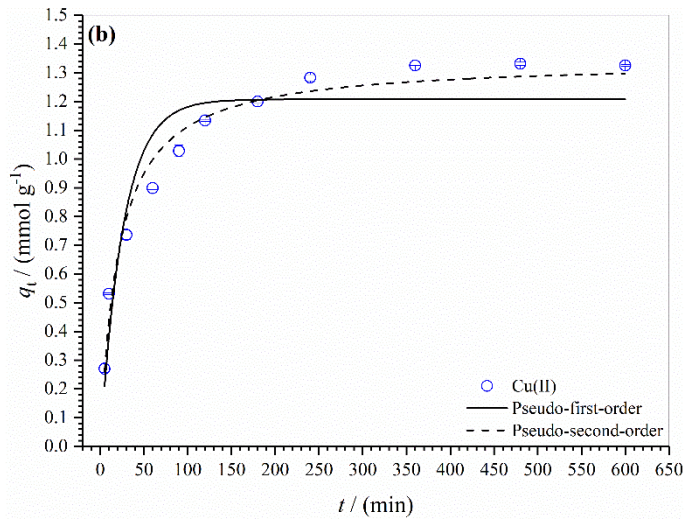
1212

1213 Figure 2d



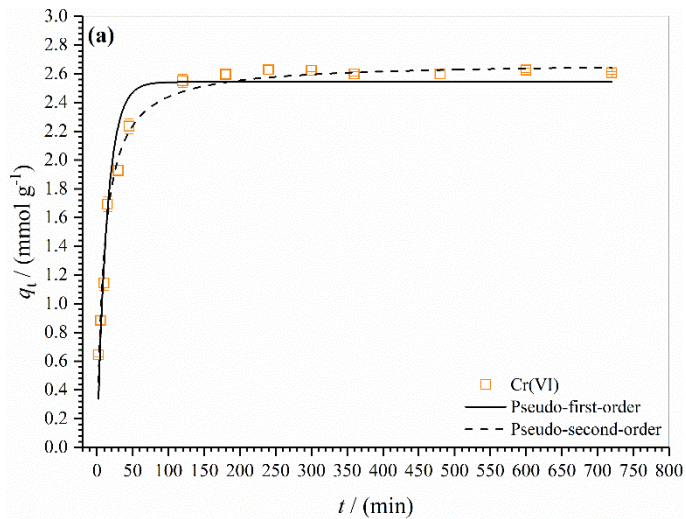
1214

1215 Figure 3a



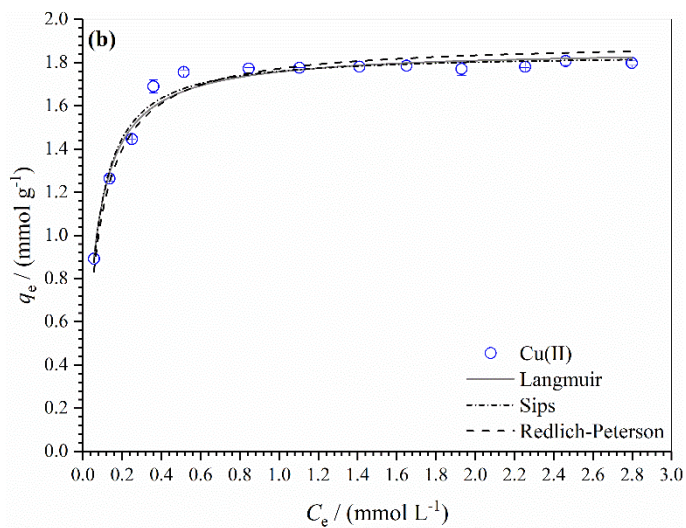
1216

1217 Figure 3b



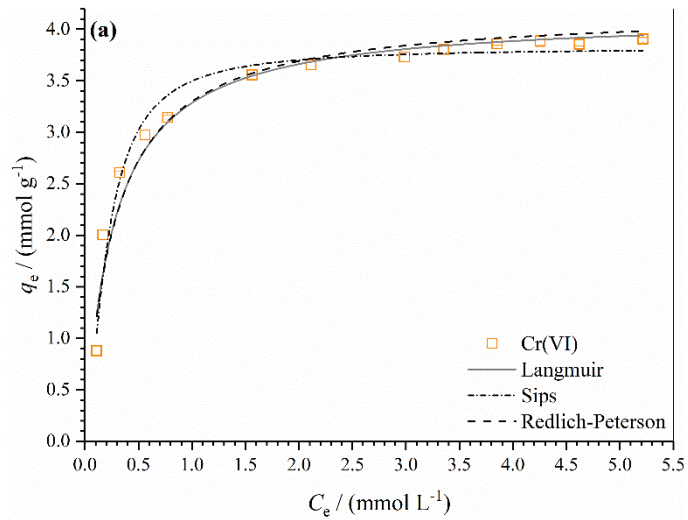
1218

1219 Figure 3c



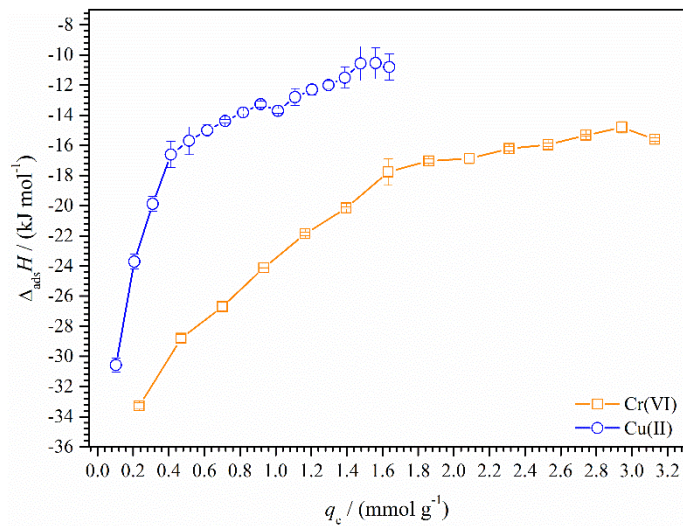
1220

1221 Figure 3d



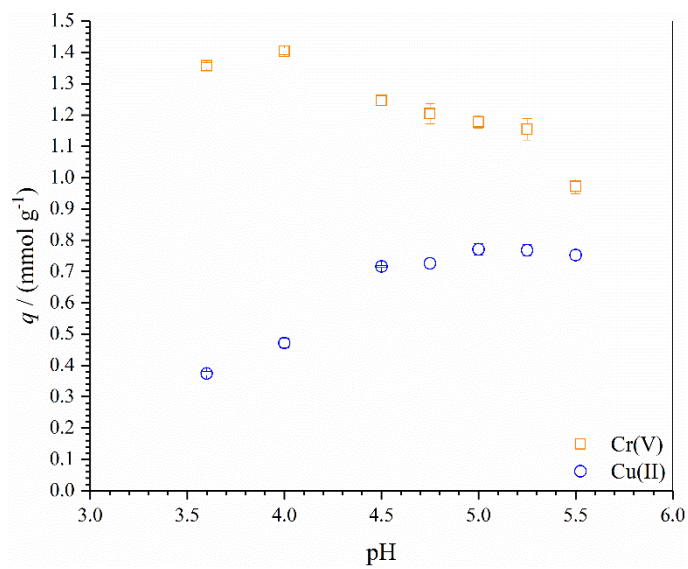
1222

1223 Figure 3e



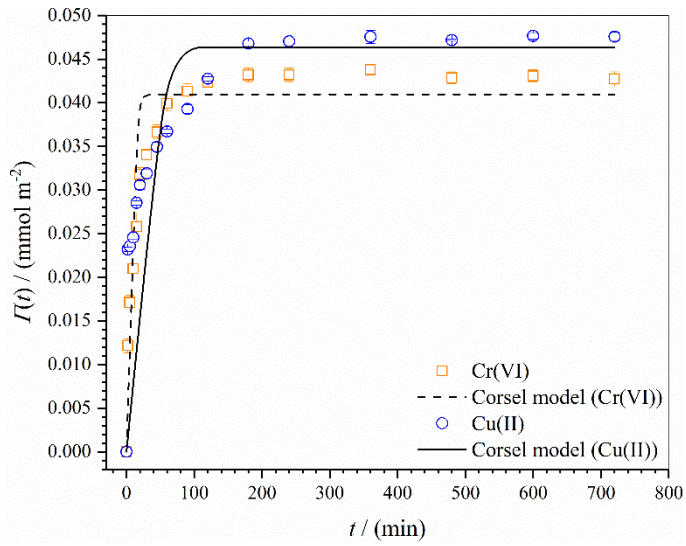
1224

1225 Figure 4



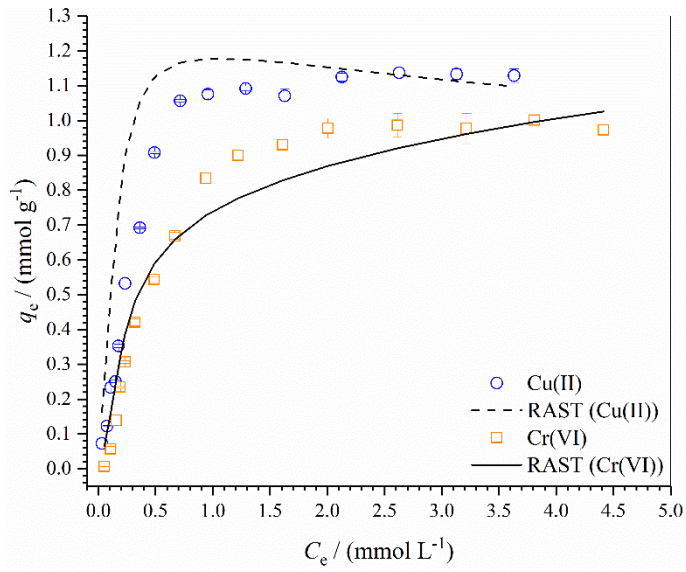
1226

1227 Figure 5a



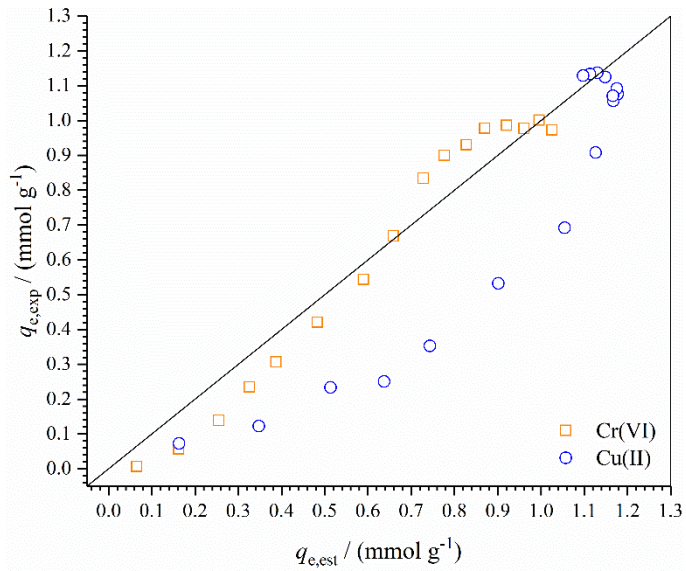
1228

1229 Figure 5b



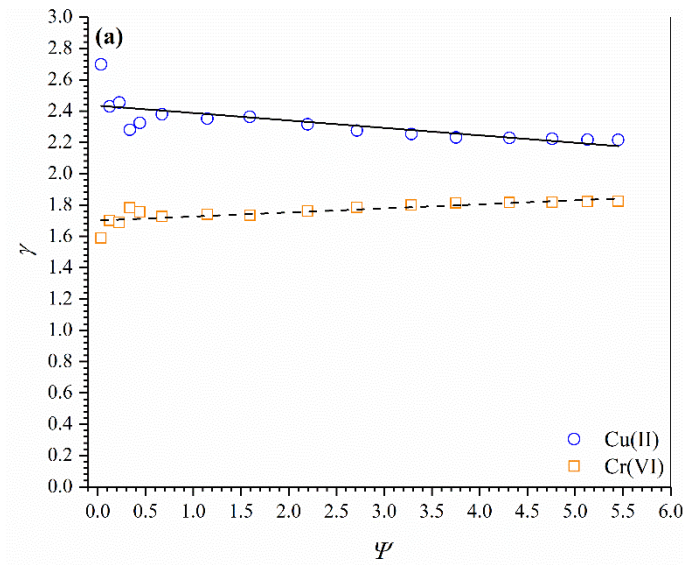
1230

1231 Figure 5c



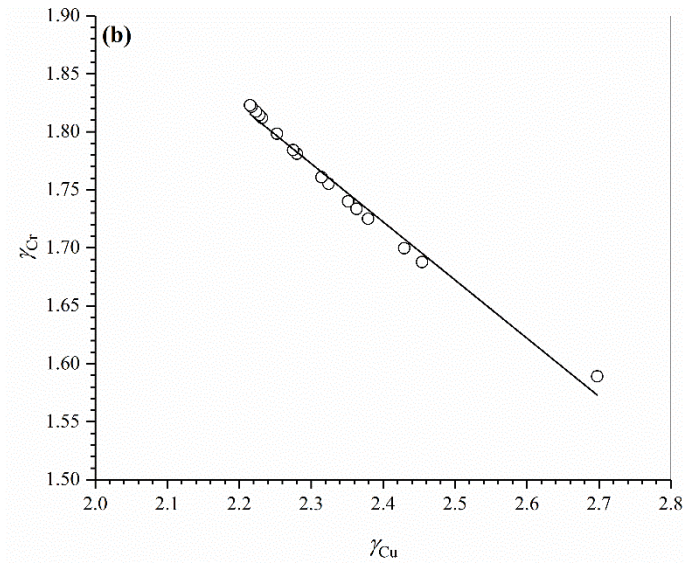
1232

1233 Figure 6a



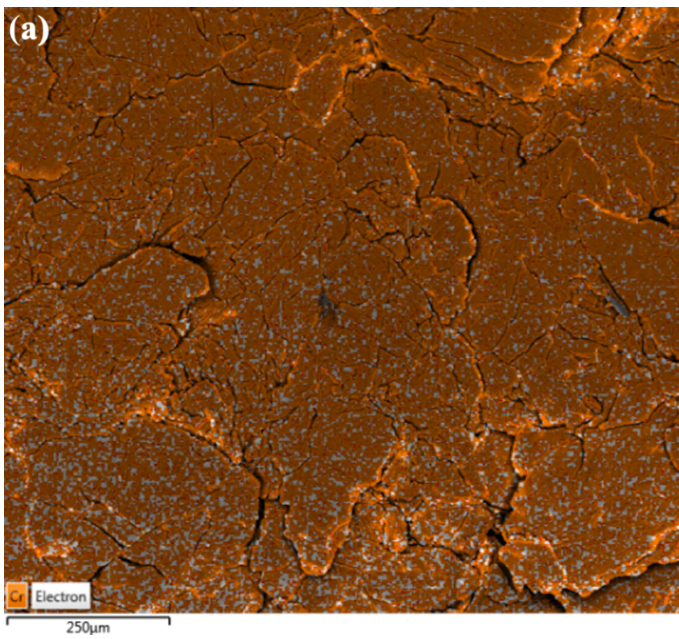
1234

1235 Figure 6b



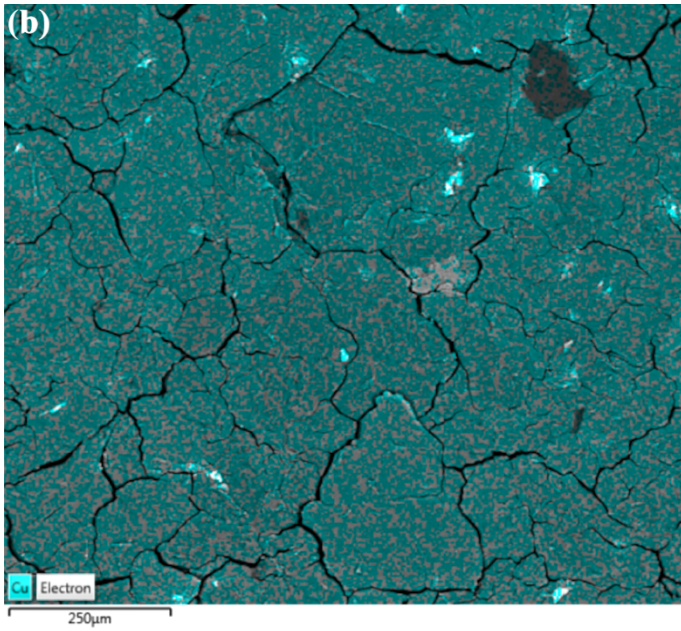
1236

1237 Figure 6c



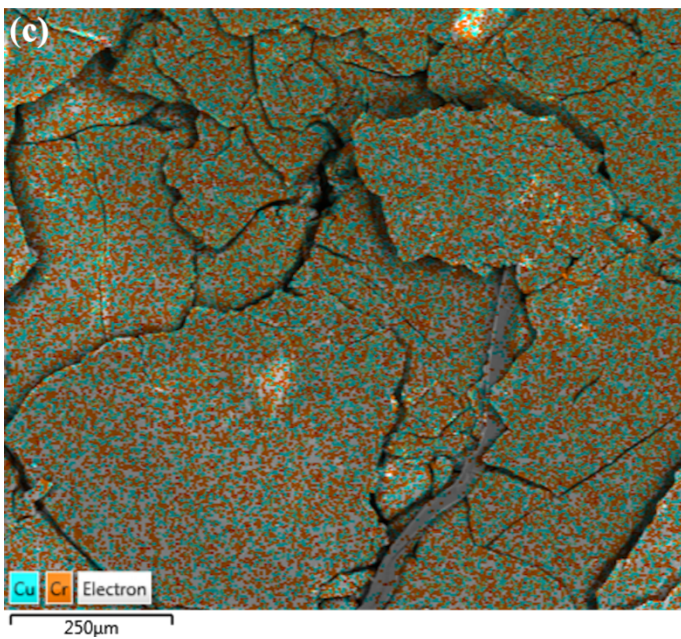
1238

1239 Figure 7a



1240

1241 Figure 7b



1242

1243 Figure 7c

1244

1245